UNIVERSITAT POLITÈCNICA DE VALÈNCIA

# UNIVERSITAT POLITÈCNICA DE VALÈNCIA

## School of Industrial Engineering

## Development of a biodegradable elastomeric patch for the treatment of chronic wounds

Master's Thesis

Master's Degree in Biomedical Engineering

AUTHOR: Tessari, Leonardo

Tutor: Vilariño Feltrer, Guillermo

Cotutor: Martín Cabezuelo, Rubén

External cotutor: GAGLIANO, ONELIA

Experimental director: SOTO PRADO, ALEXANDRA

ACADEMIC YEAR: 2023/2024

# Acknowledgement

The first person I would like to thank for the infinite support, patience and friendship is Alex, my experimental tutor with whom I worked side by side for three months. I probably couldn't have completed this thesis as well without her.

I would also like to thank my tutors, Guillermo and Rubén, who have allowed me to work with them and introduced myself to the world of scientific research.

Finally, I express my full gratitude to those who have been close to me during these months abroad, thanks to whom they have unfortunately flown too quickly. These are my roommates, the friends I met here and the friends who supported me from Italy.

Finally I cannot fail to mention my family who has always been available for anything from afar.

# Abstract

Skin is the largest and heaviest organ in the human body. It provides many vital functions for people, such as defence against pathogens agents, thermic regulation, mechanical sensor and many others. In most cases of disease, it can regenerate itself thanks to the cooperation of the factors involved in wound healing, while the cure can be insufficient under certain conditions and bacteria could penetrate the wound and proliferate. These can lead to the formation of biofilms, under which pathogens are protected from antibiotics and can damage the biological environment.

The Universitat Politècnica de València and the CY Cergy Paris Université are working in a project called THERAPATCH, that has the purpose to create a bandage containing molecules able to manage and improve the inflammatory response and provide biofilm bacteriophages, effective against these bacteria. This thesis focuses on the production of a scaffold and of an hydrogel able to contain these forementioned biomolecules, presenting characteristics like biocompatibility and biodegradability.

The polymer chosen is poli(glycerol sebacate) (PGS), a novel material that awakened a lot of interest in biomedicine for its versatile characteristics. The scaffolds will be produced by applying two different techniques. In the first, PGS is mixed with a salt mould to obtain a porous structure taking advantage of the size of the salt crystals. The second technique will use electrospinning, to obtain a scaffold formed by microfilaments arranged in a porous membrane of polymer.

Subsequently hydrogel based on hyaluronic acid or poly(vinyl alcohol) will be injected through the polymeric structure with pores and subsequently characterized mechanically.

**KEYWORDS**: Chronic wound; poly(glycerol sebacate); dermal patch; biofilm; scaffold; electrospinning.

# Resumen

La piel es el órgano más extenso y pesado del cuerpo humano. Proporciona múltiples funciones vitales, como defensa contra agentes patógenos, regulación térmica, sensación táctil y otros. Con frecuencia, ante una enfermedad puede revertir el daño de manera autónoma gracias a la cooperación de diferentes factores implicados en el curado, pero bajo circunstancias específicas, la regeneración tisular puede verse comprometida, y organismos como bacterias pueden alojarse indefinidamente en la zona. Esto provoca la formación de biofilms, en los cuales los microorganismos patógenos se protegen con más eficacia de la acción de antibióticos, y que descomponen el equilibrio biológico del entorno.

La Universitat Politècnica de València y la CY Cergy Paris Université están colaborando en el contexto de un proyecto llamado THERAPATCH, que tiene el objetivo de obtener un apósito que contenga, por un lado, moléculas bioactivas capaces de resolver la respuesta inflamatoria crónica de la herida y, por otro, bacteriófagos eficaces contra bacterias presentes, capaces de penetrar en los biofilms. Este Trabajo Final de Máster se centra en la obtención del andamiaje del apósito, y del hidrogel que albergará estas biomoléculas, con el foco en la biocompatibilidad y el perfil de liberación desde los mismos.

El polímero escogido es poliglicerol sebacato (PGS), un material con aplicación relativamente reciente en biomedicina que ha despertado mucho interés por sus características. Se pretenden evaluar dos técnicas para la obtención de estos andamiajes. Por un lado, se mezcla PGS con cristales de sal para obtener un constructo poroso, con bóvedas del tamaño de los granos. La segunda técnica se basas en electrohilado, para formar una membrana basada en filamentos de polímero distribuidos de manera aleatoria.

Por su parte, el hidrogel correspondiente, basado en ácido hialurónico o polivinil alcohol, se inyectará y gelificará en su interior, y se realizarán ensayos mecánicos para caracterizar el conjunto.

**PALABRAS CLAVE**: Herida crónica; poli(glicerol sebacato); parche dérmico; biofilm; andamiaje; electrohilado.

# Resum

La pell és l'òrgan més extens i pesat del cos humà. Proporciona múltiples funcions vitals, com a defensa contra agents patògens, regulació tèrmica, sensació tàctil i altres. Amb freqüència, davant una malaltia, pot revertir el mal de manera autònoma gràcies a la cooperació de diferents factors implicats en el curat, però sota circumstàncies específiques, la regeneració tissular pot veure's compromesa, i organismes com a bacteris poden allotjar-se indefinidament en la zona. Això provoca la formació de biofilms, en els quals els microorganismes patògens es protegixen amb més eficàcia de l'acció d'antibiòtics, i que descomponen l'equilibri biològic de l'entorn.

La Universitat Politècnica de València i la CY Cergy Paris Université estan col·laborant en el context d'un projecte anomenat THERAPATCH, que té l'objectiu d'obtindre un apòsit que continga, d'una banda, molècules bioactives capaces de resoldre la resposta inflamatòria crònica de la ferida i, d'altra, bacteriòfags eficaços contra bacteris presents, capaços de penetrar en els biofilms. Este Treball Final de Màster es centra en l'obtenció de la bastida de l'apòsit, i de l'hidrogel que albergarà estes biomolècules, amb el focus en la biocompatibilitat i el perfil d'alliberament d'estos.

El polímer triat és poliglicerol sebacat (PGS), un material amb aplicació relativament recent en biomedicina que ha despertat molt d'interés per les seues característiques. Es pretenen avaluar dues tècniques per a l'obtenció d'estes bastides. D'una banda, es mescla PGS amb cristalls de sal per a obtindre un constructe porós, amb cavitats de la grandària dels grans. La segona tècnica es basa en electrofilat, per a formar una membrana basada en filaments de polímer distribuïts de manera aleatòria.

Per part seua, l'hidrogel corresponent, basat en àcid hialurònic o polivinil alcohol, s'injectarà i gelificarà en el seu interior, i es realitzaran assajos mecànics per a caracteritzar el conjunt.

**PARAULES CLAU**: Ferida crònica; poli(glicerol sebacat); embenat dermic; biofilm; bastidor; electrofilat.

# Contents

# List of Figures

# Part I

# WORK REPORT

# Chapter 1

# INTRODUCTION

## 1.1 The skin

### *1.1.1 What is the skin?*

The skin is the largest and primary protective organ of our body [1]. It serves as first great barrier against the external environment, and its importance is key for our survival.

Its structure is a complex matrix composed by cells, nerves, hair, glands, fibres and other biomolecules that work in synchrony to provide the perfect operating of its functions. It is divided in three main layers (fig. 1.1a):

- *Epidermis*: the most external and thinnest layer. It is composed by different cells, the most of which are keratinocytes, that provides water barrier, protection against UV rays, antigen defence and light touch sensitivity [2];

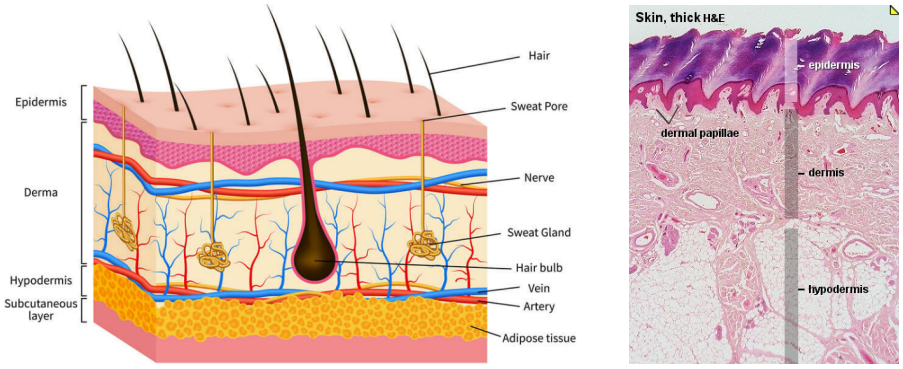


**(a)** A scheme of the skin layers. **(b)** Hystology of the skin.

**Figure 1.1:** Structure of human skin.

- *Dermis*: the middle layer, it is mainly made of fibres, ground substance and blood vessels, other than sweat glands and receptors. It gives the skin its mechanical properties and temperature protection [3];
- *Hypodermis*: mainly composed of fat and connective tissues, it functions as energy source and impact pad [2].

Defence is a critical role that is brilliantly performed thanks to the cooperation of the skin environment: it does not concern only bacteria and other pathogens, but also protection to UV rays, chemical substances and mechanical damage.

Body protection is not the only task of the skin[1]. Other functions include:

- **sensation**: pain, temperature, touch, pressure;
- **mobility**: permits smooth movements of the body;
- **endocrine activity**: synthesis of vitamin D from sunlight;
- **exocrine activity**: release of pheromones and bioactive substances;
- **regulation of temperature**: thanks to the lipid sheet in the skin, its ability to transpire and the ability of sweat to regulate the thermic flux.

In case of wound, come into play a series of efficient healing processes that pass through four phases: hemostasis, inflammatory, proliferative and remodeling [4].

Briefly, the first phase is the fastest one, it takes few hours, and we have the creation of a platelet plug. It serves to avoid the loss of blood outside the veins. At the same time the inflammatory response starts. It is the physiological response that occurs when the natural continuity of the human tissue breaks. Macrophages, platelets, antibodies and other components approach the damaged site to eliminate foreign bodies (*foreign body's response*) and to clean the site from injured or harmful elements. In the proliferative phase, fibroblast and other cells tries to reconstruct a first functional environment, but the remodeling, namely the modeling of the original tissue, will require a lot of time, even months or years. The purpose of this phase is to achieve the maximum tensile strength through reorganization, degradation, and resynthesis of the extracellular matrix [5].

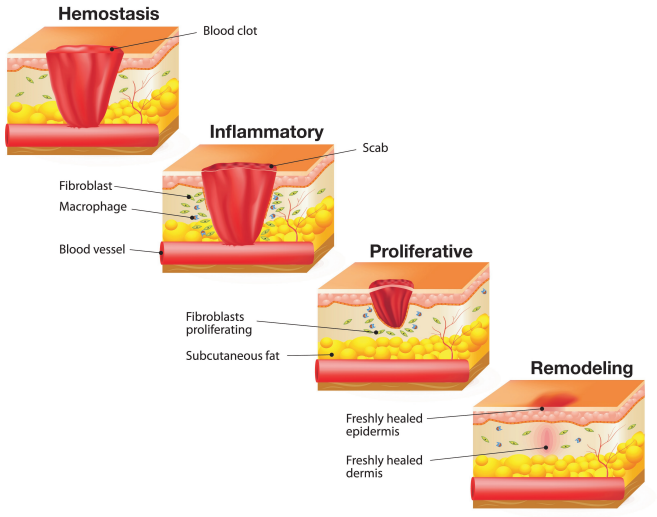


**Figure 1.2:** Healing process phases.

### *1.1.2 Skin diseases*

In case of wound, after an injury, skin can naturally heal. However, under conditions, it may slow consistently the healing time or bring to a chronic disease. Factors that may interfere with the curing process can be divided into local and systemic factors [6]. Local factors are: oxygenation, infections, foreign bodies and venous sufficiency, and are the ones that are present in the specific zone of the disease; systemic factors that concern the entire body and are age, gender, hormones, stress, ischemia, diseases, medications, among others.

It is now recognized that the proliferation of bacteria into the wound tends to compromise the healing process. This subsequently allows the formation of biofilms, which correspond to communities of microorganisms that are embedded into matrix of extracellular polymeric substances (EPS).

A biofilm is an assemblage of microbial cells that is irreversibly associated with a surface and enclosed in a matrix of primarily polysaccharide material [7]. Within the biofilm, bacteria are cocooned in a self-produced extracellular matrix, composed of EPS. Inside the host, the matrix protects biofilm bacteria from exposure to innate immune defense (such as opsonization and phagocytosis) and antibiotic treatments [8],[9],[10]. Interbacterial interactions can promote the spread of drug-resistance markers and other virulence factors [11]. As consequence, not only the healing time is slowed, but could also lead to chronic wound and a subsequently risk of additional infections.

The Global Burden of Disease project has shown that skin diseases continue to be the 4th leading cause of nonfatal disease burden world-wide [12]. Additionally, it reveals variation by age, with infections of skin condition causing greater burden among children; variation by gender, pigmentary disorders, certain hair diseases, and particularly autoimmune as well as allergic diseases [13].

All these premises lead us to seek a solution with the purpose of promoting the skin regeneration, including the removal of chronic wound factors, like biofilms.

## 1.2 Current research therapies for chronic wounds

Commercial wound healing skin dressings, such as Hartmann's Hidrocoll [14], are based on a self-adhesive, absorbent fabric with a high absorption capacity that is covered with a semi-permeable membrane. Because of the semi-permeable polyurethane layer, they keep the wound moist and aid in healing while limiting bacterial penetration.

In order to facilitate the efficient delivery of loaded medications into the target area and prevent excessive adhesion between the skin and the patch, the majority of the strategies put forth in the literature to address the antibiotic resistance crisis are quite recent. We can now quote Donnelly's work, which is currently on clinical trials in humans [15]. Sotiriou [16] suggests a microneedle array with a water-insoluble support layer for the regulated topical administration of vancomycin, a drug whose large molecular weight makes transdermal penetration impossible. Wang [17] has created a biomass chitosan microneedle array (CSMNA) patch coupled with smart responsive medication delivery as a more sophisticated approximation. Furthermore, temperature-sensitive hydrogel encapsulates vascular endothelial growth factor in the micropores of CSMNA. As a

result, the temperature rise brought on by the inflammatory reaction at the site of wounds can be used to controllably allow the smart release of the medications. Photothermal irradiation is another, less common, method of infection prevention [18]. The skin patch combines reduced graphene oxide nanosheets for laser-gated pathogen inactivation with the near-infrared photothermal characteristics of a gold nanohole array created by self-assembly of colloidal structures on flexible polyimide films.

Finding innovative, inexpensive, safe compounds to treat infectious, neoplastic, and inflammatory skin diseases is of increasing interest to the medical community. Recent studies indicates that curcumin might be a useful treatment for a number of skin disorders [19]. It has been applied to the treatment and chemoprevention of psoriasis, scleroderma, and skin cancer [20]. It has been demonstrated that curcumin protects skin by scavenging free radicals and lowering inflammation by blocking nuclear factor-kB. Additionally, curcumin therapy sped up the healing process, enhanced collagen deposition, and boosted fibroblast and vascular density in wounds, improving both healthy and damaged wound healing. Additionally, curcumin has been demonstrated to be useful as a proangiogenic agent in wound-healing through the induction of transforming growth factor-b, which in turn promotes angiogenesis and extracellular matrix buildup that persists into the remodeling stage of wound repair. In particular, a number of clinical trials are currently underway to investigate the topical administration of curcumin in the form of chitosan-alginate sponges, foams, or collagen films, as well as a hydrogel system containing curcumin micelles, chrysin-curcumin-loaded nanofibers, or curcumin-loaded chitosan nanoparticles impregnated into collagen-alginate scaffolds [19].

The most effective approach for utilizing lytic bacteriophages as a therapeutic treatment for pathogenic bacterial skin infections, especially those caused by multiple antibiotic-resistant bacteria, is likely through topical administration. This method allows direct access to the infection site while circumventing the systemic immune response of the host. Topical (as opposed to intravenous (IV)) administration may be the most practical, economical, and safest method of delivering phages. It can be applied directly, impregnated into innovative dressings, or encapsulated in a variety of media (such as hydrogels). On the other hand, IV phage administration might be necessary for systemic infections and to reach bacteria that have been sequestered in deep tissue recesses and are not reachable by isolated topical delivery [21].

Studies conducted up to the present day used hydrogel dressings to impregnate the phages. If not, the phages are suspended in phosphate-buffered saline and then impregnated in bandages or filter paper discs. A poly(ester amide) is impregnated with a phage cocktail in PhagoBioDerm [22], a commercial dressing licensed in the Republic of Georgia. The dressing is reapplied as needed upon degradation of the polymer and ongoing wound healing requirements. This method has demonstrated improvement in radiation-induced cutaneous ulcers that are secondary to infection as well as infected venous stasis ulcers. A phase 1/2 clinical trial in [23] successfully tested an alginate dressing for burn-mediated wound infections (PhagoBurn). Based on these results, topical phage therapy in conjunction with hydrogel-mediated curcumin administration appears to be a safe, promising, and potentially game-changing treatment option for stubborn infectious cutaneous wounds.

Furthermore, over the past five years, there has been an acceleration in the development of materials that promote wound healing-not for topical phage therapy, but as hemostatatics. Various

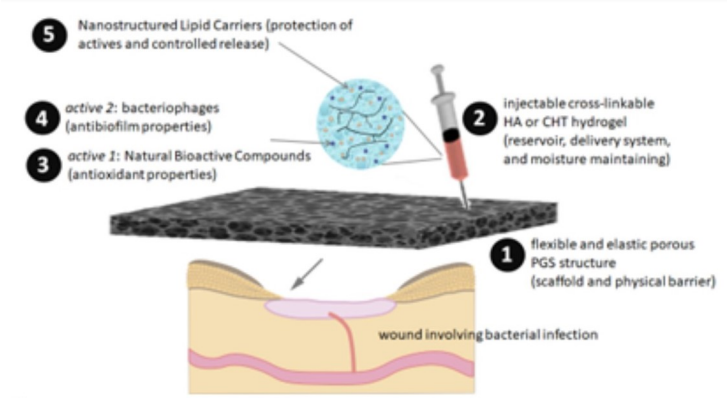


**Figure 1.3:** Scheme of the multiscale system proposed to address skin wounds and pathologies that can evolve with bacterial contamination, with its components for (1) protection, (2) hydration and controlled release of active agents, (3) anti-inflammation and (4) phagotherapy.

forms (such as sponges, hydrogels, nanofibres, and particles) and compositions of natural and synthetic polymers, silicon-based materials, metal-containing materials, and other components have been used to create a multitude of hemostatic materials [24].

### *1.2.1 The* THERAPATCH *project*

In lights of these studies, the Centre for Biomaterials and Tissue Engineering at the Universitat Politècnica de València in collaboration with the Equipe de Recherche sur les Relations Matrice Extracellulaire-Cellule at the CY Cergy Paris Université are working in a project called *THERAPATCH*. The purpose is to create a dermal patch to apply directly on the wound that will release pro-healing biomolecules. The idea is to create a dual patch made up of an elastomeric bandage and a hydrogel containing a combination of actives: a natural bioactive compound and bacteriophages, with antioxidant and antibiofilm properties, respectively.

The choice of all these materials will bring benefit from different points of view (fig.1.3):

1. Protection: the application of the bandage directly on the wound will act as a physical barrier between the lesion and the external environment;
2. Structure: a flexible elastomeric polymer will easily adapt to the surface of the wound and to the movement of the skin;
3. Confinement: an hydrophobic polymer will trap in its environment the hydrogel to maintain moisture in the damaged tissue;
4. Hydration and release: the hydrogel will keep the tissue hydrated and will release biomolecules in a controlled way;
5. Heal: elimination of pathogens and tissue repair, i.e., the final purpose.

Thus, it becomes mandatory to determine which materials, chemistries and combined structures are the best suite for the release of these bioactives components and best interact with cells involved in the inflammatory and regenerative process of the skin. The work of this thesis is part of this project, in particular in the development of a scaffold and a hydrogel able to meet these requirements.

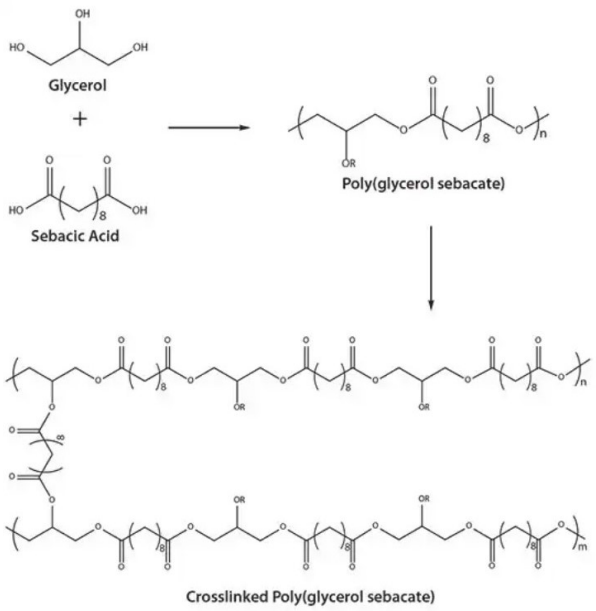


**Figure 1.4:** Synthesis of PGS. From reagents to the cross-linked polymer. Image extracted from [26].

## 1.3 PGS

Poly(glycerol sebacate), better known with the acronym PGS, is a novel polymer synthesized for the first time by Wang in 2002 [25]. There is an increasing consideration of this polymer in the research world due to its chemical and mechanical properties, biocompatibility, biodegradability, cost and ease of creating.

The polymer is the result of a condensation reaction between glycerol and sebacic acid. Both have received approval from the U.S. Food and Drug Administration in the medical field, increasing its interest in the field of biomedical engineering.

The reaction takes place in two phases. In the first, through a pre-policondensation process, a white and waxy prepolymer is formed, while in the second crosslinking occurs, providing a polymer whose characteristics depend on the mode of preparation.

### *1.3.1 Properties*

Understanding the properties of any biomaterial in depth is the first step towards elucidating its potential for possible applications (a complete review of PGS has been done by Ray in [27]). However, the PGS presents a lot of characteristics varying due to many procedure parameters. These are the molar ratio, the temperature of curing, the curing time, the pre-polymerisation atmosphere and many others [28],[29],[30]. Excellent examples are found in Conejero-Garcia and Li's work ([29],[31]). In fig. 1.5, extracted from Li's work, in which the degree of esterification is proposed as method to compare the degree of curing, we can appreciate the behaviour of the obtained polymer in dependence n curing temperature and time.

It is hydrophilic and therefore promotes the development of scaffolds capable of retaining hydrogels, useful in biomedicine. In addition, although the mechanical properties are variable, it typically behaves as an elastomer, allowing it to be used for controlled drug release.

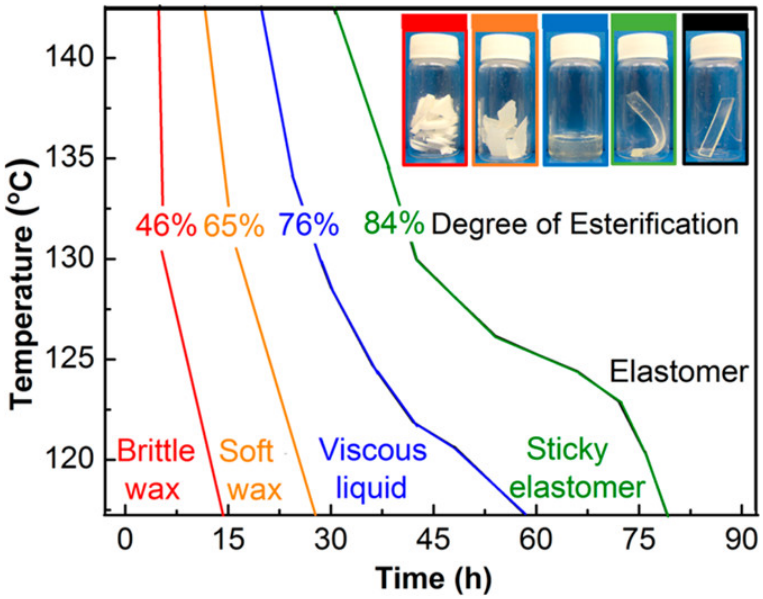


**Figure 1.5:** In this paper Li proposed the measurement of the degree of esterification of PGS as method to compare the curation degree. These lines show that different methods combined with different hours of curation lead to a various range of doe. Image extracted from [31].

Another important property is biodegradability. It has been demonstrated in the work of Wang [32], in an experiment with Sprague-Dawley rats, that PGS degrades linearly to total body absorption, fig. 1.6. This, together with its biocompatibility, makes it an excellent biomaterial for tissue engineering.

### *1.3.2 Applications*

For the characteristics described above, PGS is capturing a lot of attentions in biomedical engineering. The fields of biomedicine in which this polymer is being utilised are very numerous and for a detailed and well exposed list [27] and [33] are good reviews. Briefly, its main uses are found in the following examples:

In cardiac tissue engineering its used as a patch to deliver healthy cardiac cells onto the infarct region and provide left ventricular restrain. In vascular tissue engineering they are trying to construct PGS based blood vessels (fig. 1.7a). The mechanical properties of PGS are such as to possibly replace the cartilage tissue and they are trying to build a PGS scaffold to substitute it in case of necessity. Another use is found in retinal tissue engineering in designing and manufacturing biodegradable devices that serve as a support for retinal regeneration. In the field of nerve regeneration PGS-based constructs, such as nerve conduits or scaffolds, are designed to provide support and guidance for regenerating nerve fibers. In the context of repairing a tympanic membrane, PGS can be utilized to develop biodegradable materials for tympanic membrane grafts. PGS-based constructs offer a potential solution for creating tympanoplasty patches that can be used to repair perforations or defects in the tympanic membrane.

PGS shows promise in medical applications, particularly as a barrier material to prevent visceral peritoneal (VP) adhesions and as a surgical sealant. In preventing VP adhesions, PGS films demonstrated superior mechanical properties, biocompatibility, and resorbability compared to

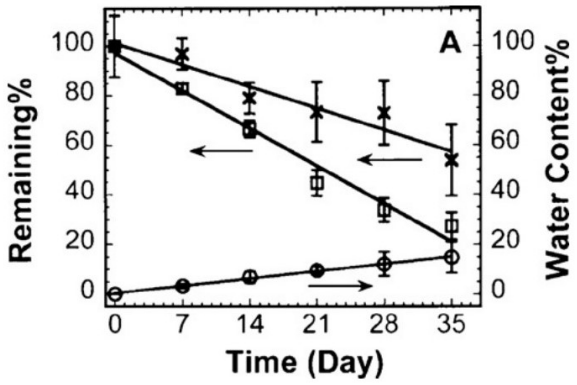


**Figure 1.6:** Biodegradability of PGS. *In vivo* degradation of PGS implants up to 35 days in young adult female Sprague-Dawley rats. Squares represent the changes in mass, crosses the mechanical strength and circles the water content. Notice that the changes are linear. Extracted from [32].

existing hyaluronic acid-based films. Additionally, PGS-co-LA, a copolymer of PGS and lactic acid, was developed as a surgical sealant with a liquid-to-solid transition.

The polyester has been explored for drug delivery applications as well. Its unique properties, such as biocompatibility and tunable degradation rates, make it an attractive candidate for controlled drug release systems. Researchers are investigating the use of PGS-based hydrogels and other formulations to encapsulate and deliver drugs in a controlled and sustained manner. This versatility in drug delivery applications underscores the potential of PGS in the pharmaceutical field (fig. 1.7b).

PGS finds versatile applications in biosensors and electrical devices owing to its unique properties. When employed in a porous and degradable form, PGS blended with carbon nanotubes and salt serves as a highly sensitive piezoresistive sensor for pressure, exhibiting enhanced electromechanical performance. Additionally, electrospun PGS-PCL mesh coated with silver offers a flexible and conductive solution for wearable electronics, enabling applications such as biocompatible heaters, temperature sensors, and wireless strain detectors for monitoring muscle tissue motion in electromyography. This adaptability positions PGS as a promising material for biomedical and healthcare innovations.

## 1.4 Hydrogels

### *1.4.1 Hyaluronic Acid*

Hyaluronic Acid (for an overview where to find the sources of this resume see Kuo *et al.* [34]) is a ubiquitous and essential component of the extracellular matrix in various biological systems. This glycosaminoglycan, also known as hyaluronan, plays a crucial role in maintaining tissue hydration, lubrication, and structural integrity. Its unique properties make it a fascinating subject of study in the fields of chemistry, biology, and medical science.

In nature, HA is found in connective tissues, synovial fluid, and the vitreous humor of the eye, where it contributes to the viscoelastic properties and lubrication of these tissues. Its presence in

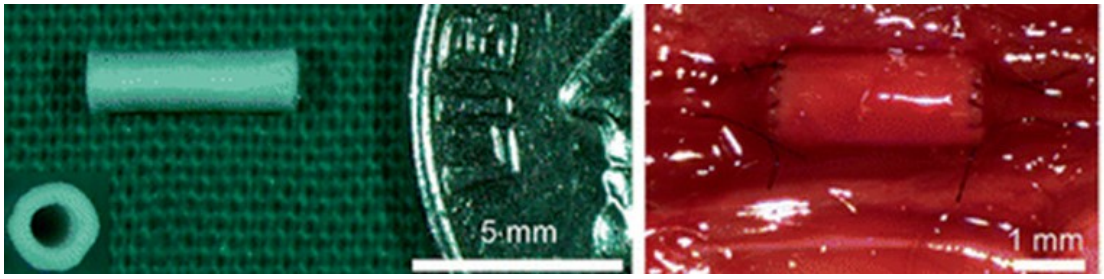


**(a)** PGS grafts in vascular tissue engineering.

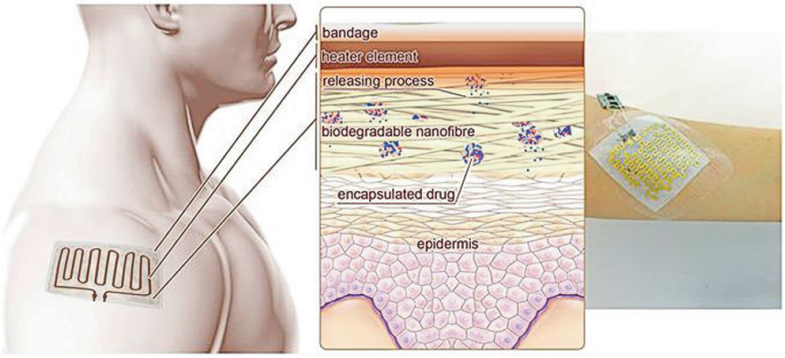


**(b)** Functional principle of a drug delivery system with integrated heating element and electronics.

**Figure 1.7:** Examples of PGS applications in biomedicine. Images extracted and adapted from [33]

these diverse biological environments underscores its significance in maintaining tissue function and homeostasis.

Chemically, HA is a linear polysaccharide composed of repeating disaccharide units of N-acetyl-glucosamine and glucuronic acid. This structure imparts HA with exceptional water-binding capacity, contributing to its viscoelastic and hydrating properties. Furthermore, HA's molecular weight and conformational flexibility play a pivotal role in its biological functions and medical applications.

HA exhibits remarkable biocompatibility, making it an ideal candidate for applications as a hydrogel in various biomedical contexts. Due to its natural presence in the human body and its non-immunogenic nature, HA is well-tolerated and does not typically elicit adverse immune responses or toxic effects. When used as a hydrogel, HA's biocompatibility allows for safe and effective interactions with biological systems, making it suitable for tissue engineering, drug delivery, and wound healing applications. Its ability to retain water and create a hydrated environment further enhances its utility as a hydrogel, providing support for cell growth and tissue regeneration. Overall, HA's biocompatibility and hydrophilic nature make it a valuable material for developing hydrogels with diverse biomedical applications.

### *1.4.2 PVA*

Polyvinyl alcohol (PVA), derived from the polymerization of vinyl alcohol monomers through the saponification of polyvinyl acetate, stands out as a synthetic polymer with unique properties in the biomedical context. Its linear and water-soluble molecular structure, characterized by orderly chains, provides flexibility and stability ideal for applications in this field [35].

From a chemical perspective, PVA, owing to its water solubility, lends itself to the production of biomedical devices and materials. This characteristic, coupled with the material's mechanical strength, makes it suitable for creating biomaterials, hydrogels, and structures that can be utilized in the medical domain.

Although not naturally occurring, PVA's versatility allows for combinations with biocompatible materials, expanding its potential in biomedical applications. This approach, combined with water solubility, contributes to enhancing the usability of PVA-based biomedical materials.

In the biomedical sectors, PVA finds applications in the production of drug delivery hydrogels, membranes for dialysis, and scaffold structures for cell growth. Its biocompatibility and moldability make it an advantageous choice for the development of advanced medical devices.

## 1.5 Approach of this thesis

This thesis aim to produce a scaffold in which insert hydrogel, in HA o PVA, that could be appropriate for the Therapatch project. The time concerning this period of studies is about four months.

A first task of this work is the study of the effect of the depth and the free-air surface of the mould in which PGS is cured.

The three-dimensionals structure will be created as a sponge-like scaffold or an electrospun-membrane (figg. 1.8a, 1.8b). In the first case, the resulting interconnected voids should be of subcellular size (a few dozens of micrometers in diameter in the spherical pores, much less in the passages between pores). The electrospinning technique results in porous membranes on a subcellular scale due to entanglement of the fibers when deposited on the collector, which leave too tortuous paths. In parallel, non-porous films will be manufactured to obtain bilayered structures, and to be used as controls. All this materials (with or without porosity) will be combined with the gels developed in Task 1.2.

Porous scaffold will be created through NaCl grains. Techniques with different conditions will be evaluated to obtain the best solution in terms of porous dimensions, distribution and inter-porous voids. These are the use of grain of various size and the polymer-salt ratio. The deposit of the salt at different pressures will be studied, other than the use of humidity and the use of nano-salt to increase the inter-porous void dimensions. Field Emission Scanning Electron Microscopy (FESEM) images will be determinant for the final evaluation.

In the framework of this project, it will be necessary to establish the procedure for the electrospinning of the PGS resin or pre-polymer, and to cure the membrane in a second step. There are a few works that describe the process, with pure PGS or combined with other polymers, but in all of them the resin is electrospun without its subsequent curing [36],[37],[38]. The idea is to

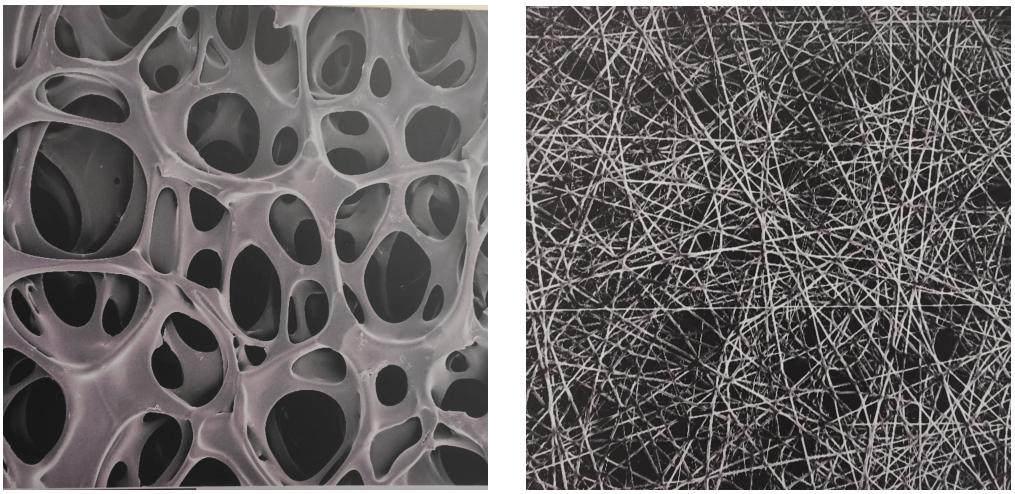

**(a)** Porous 3D scaffold. **(b)** Electrospun membrane scaffold.

**Figure 1.8:** Electron-microscopy images of the inner structure of different type of scaffolds.

dissolve the prepolymer of PGS with a solvent like ethanol and put the compound directly in the machinery for the electrospinning varying some parameters.

The project admits the creation of the hydrogel with HA and poli(vinil alcohol) (PVA). After its production, we will proceed with the insertion in the previous generated scaffolds for the evaluation of mechanical tests.

# Chapter 2

# OBJECTIVES

All the studies and experiments that will be done during these months are part of a larger project and the results will be helpful for the subsequent parts. The objective of this thesis are:

- PGS synthesis optimization: the objective is to understand if the PGS can be cured in the absence of a large surface in contact with air and this changes according to the depth of the test;;
- creation of a scaffold to be used in the future as a spongy base of a patch that releases biomolecules for wound care and disinfection:
    1. porous scaffold created by combinations of NaCl grains and polymer;
    2. PGS electrospun membrane created through the use of electrospinning technique.

# Chapter 3

# MATERIALS AND METHODS

## 3.1 General procedure for synthesis of poly(glycerol sebacate) prepolymer

Equimolar (1:1) ratio of sebacic acid (SA) (>99%, Sigma Aldrich, 202.25 g/mol) and glycerol (Gly) (99%, Sigma Aldrich, 92.09 g/mol) were measured and mixed in a round bottom flask. To obtain a total of 40 g of the compound, 27.48 g of SA and 12.52 g of Gly were used.

Then, the flask was introduced into a glass container with 2L of mineral oil and placed on a hot-plate stirrer. The plate had a rod temperature probe that was introduced into the oil bath to monitor its temperature. Two stirring magnets were introduced, one inside the reaction flask to homogenize the mixture of both reagents and the other inside the oil bath, to facilitate the distribution of the heat flow coming from the heating plate. In addition, the glass container containing the oil was covered with aluminium to minimize heat loss to the surroundings. At the moment of the deposit of the flask in the oil bath, the temperature was set at 140°C and immediately changed to 130°C and 250 rpm of stirring velocity when the SA is molten, under a nitrogen flux (figs. 3.1, 3.2a and 3.2b).

After 24 hours at that conditions, it was removed from the oil bath and poured in a small glass container, while it was still liquid. When not used, it was kept in a refrigerator at 4°C.

## 3.2 Preparation of PGS films

The control sample for FTIR and DSC analysis was prepared in a 1 mm thick Teflon® sheet cut with a cutter to obtain a squared mould of side 3.4 cm and a total volume of 1.156 $cm^3$. Then, the mould was placed on glass plate and both were put on a scale that was calibrated. Subsequently 1.5 g of prepolymer was weighted and spread into the cavity. Four clamps, one for each side, were used to pressure the glass against the sheet to avoid the leakages of prepolymer

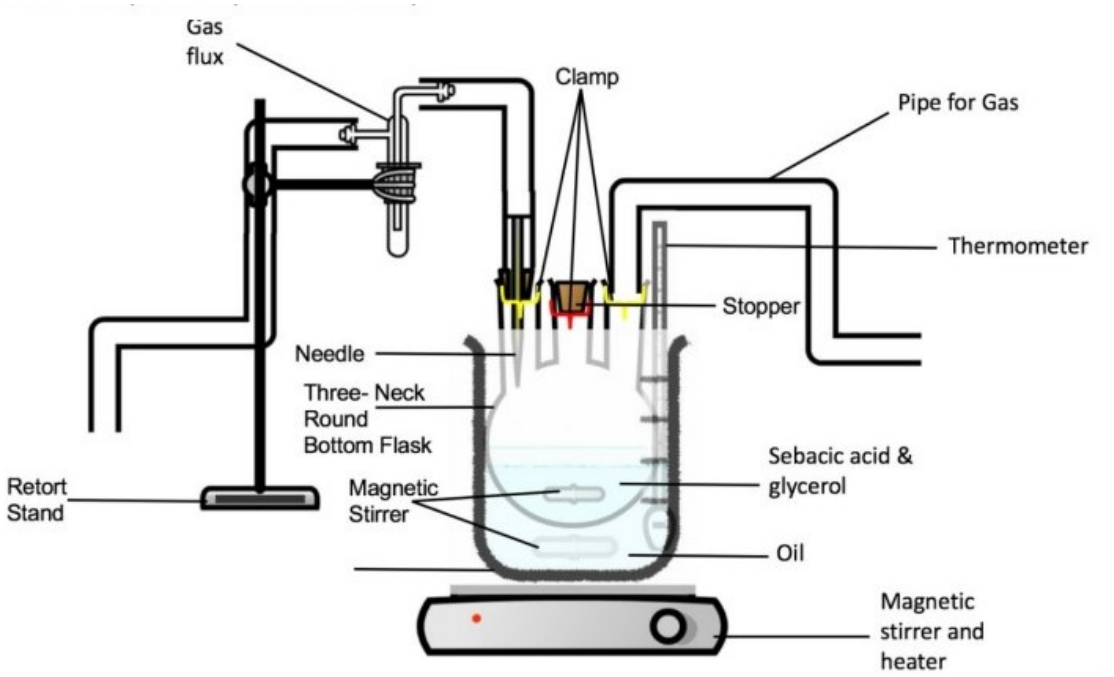


**Figure 3.1:** A scheme of the setup where SA and Gly cook and become pPGS. Image extracted from [30].

**(a)** SA and Gly mixed in the flask, getting immersed in the oil.

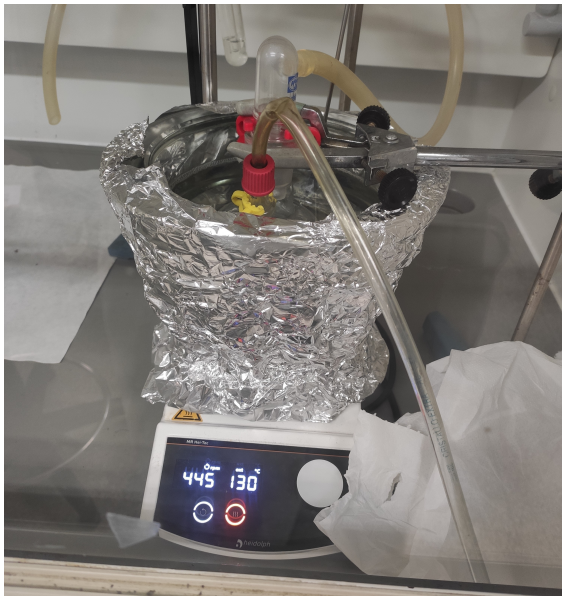


**(b)** Setup of the first phase of the prepolymer.

**Figure 3.2:** Preparation of PGS prepolymer.

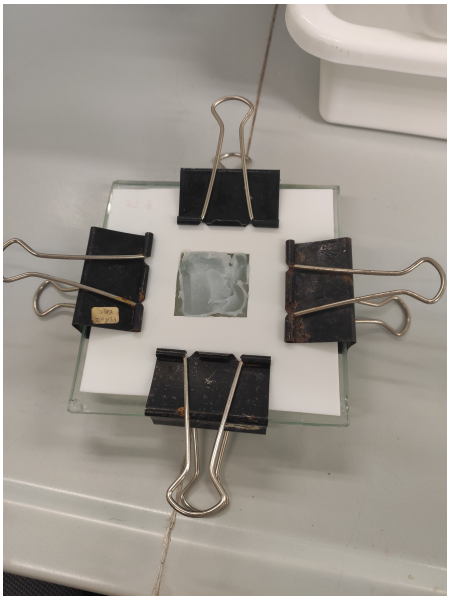

**(a)** Prepolymer inside the mould a moment before being put in the oven to create a squared 1 mm high film.

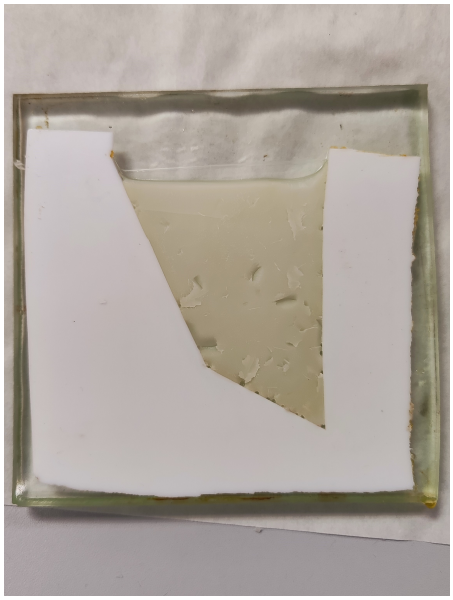

**(b)** Example of a vertical mould with PGS inside.

**Figure 3.3:** Preparation of PGS films.

during the curing 3.3a. Finally, it is proceeded with the curing in a oven for 48 hours at 130°C. The removal of the film from the mould was performed with a blade and the help of ethanol.

The PGS film for mechanical analysis was produced in the same way, but using a cylindrical Teflon mould with inside a cylinder-shaped cavity of 4 cm diameter. In that case 4.89 g of prepolymer were placed in to create a 3 mm PGS layer.

### *3.2.1 Films for reproducibility tests*

Given the immense number of variables that can affect the characteristics of PGS, five PGS films have been produced in series, all with the same conditions, to study the reproducibility of the process. As the only difference we used smaller squared 1 mm high moulds with $1 \times 1 \times 2$, for a total of 2 $mm^3$ and a PGS mass of 0.52 g. The curing time was 24 hours. These samples were compared through DSC, FTIR tests.

### *3.2.2 PGS films for confined volume test*

For this experiment a 2 mm thin and 8 cm high Teflon mould was used. The mould was placed between two glass plates and disposed vertically. Then, 8.5 g of prepolymer were poured inside through the narrow opening, that represent the only air surface in contact with pPGS. The bottom was oblique to allow samples taken at different heights to be all in the same condition of contact with Teflon, fig.3.3b. Finally, it was cured in the oven for 48 and for 72 hours.

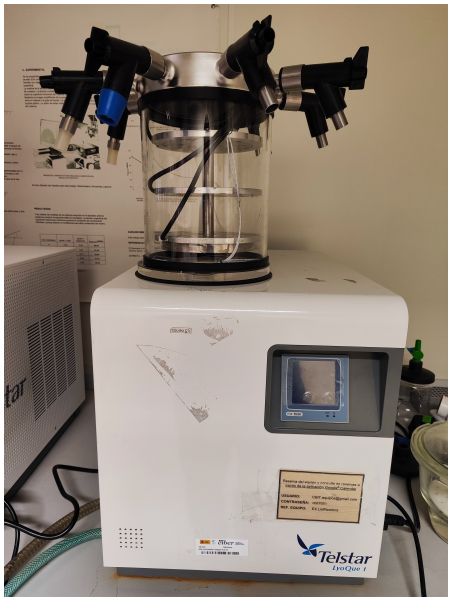


**Figure 3.4:** Images from the confined curing test.

## 3.3 Freeze-Drying

Freeze-Drying was applied to pPGS in one test of confined volume test to remove through sublimation as more water absorbed by PGS during condensation as possible to accelerate the curing process. The freeze drier was Telstar LyoQue t, fig. 3.4. The prepolymer was left for three days at −80°C in vacuum at 10 mBar.

## 3.4 Differential Scanning Calorimetry

Differential Scanning Calorimetry (DSC) is a thermal analysis technique used in material science and chemistry to investigate the heat flow associated with phase transitions, chemical reactions, and thermal events in a sample. The primary purpose of DSC is to measure the heat absorbed or released by a sample as it is subjected to a controlled temperature program. DSC operates by comparing the heat flow to or from the sample and a reference material as both are subjected to the same temperature profile. Any difference in heat flow between the sample and reference is indicative of a change in the sample's thermal behaviour. This technique provides valuable insights into the thermodynamic properties and stability of materials, making it a powerful tool for characterizing polymers, pharmaceuticals, and various other substances.

DSC was done with Perkin Elmer DSC 8000 (fig. 3.5a) and the crystallization temperatures were compared. The quantities of cured PGS put inside the machine were between 3 and 5 mg. The cycle began at 50 degrees, increased by 20°C per minute to 150°C, remaining at that temperature one minute. Then it went down to -50°C, at −20°C/min, remaining there five minutes, and then back to 150°C, always with the same temperature ramp. The step analysed was the last, the heating from -50°C to 150°C. In particular, The fusion temperature ($T_f$) was determined for each of the samples from its calorimetric curve and compared to esteem a curing grade.

**(a)** Perkin Elmer DSC 8000

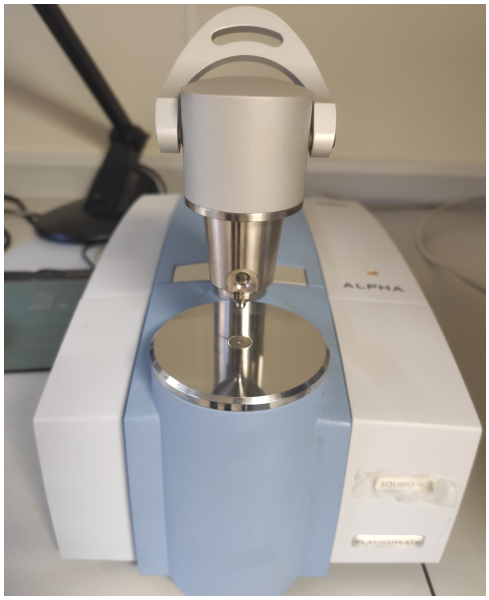


**(b)** Bruker ALPHA Platinum ATR

**Figure 3.5:** Laboratory devices.

## 3.5 Fourier Transform Infrared Spectroscopy

Fourier Transform Infrared Spectroscopy (FTIR) is a powerful analytical technique used in chemistry and materials science to identify chemical compounds based on their infrared absorption or emission spectra. FTIR spectroscopy operates on the principle that molecules absorb specific frequencies of infrared light that are characteristic of their chemical structure. In FTIR, a sample is exposed to infrared radiation, and the resulting absorption spectrum is measured. The Fourier transform technique is then applied to convert the data from the time domain to the frequency domain. This transformation enhances the accuracy and speed of data acquisition compared to traditional methods.

FTIR test were carried out with a Bruker ALPHA Platinum ATR (fig. 3.5b) and the spectra resulted from averages of 48 scans at a resolution of 4 $cm^{-1}$, between 400 and 4000 $cm^{-1}$. The spectral data were expressed in transmittance, for easy comparison between samples. The $-OH/-COOH$ and the $-OH/-COOR$ peaks were compared as estimation of the curation grade.

## 3.6 NaCl sieving

A mixture of different grain size of NaCl was used. The goal was to obtain the largest amount of salt sifted in the most precise way possible. With a scale it was possible to weight different quantities from 10g to 100 g. Using a mortar, the salt was ground to break up potential moisture-related lumps.

Sieving took place by stacking sieves with lumens ranging from 400 $\mu$m to 106 $\mu$m. The sieves were stacked from top to bottom in descending order. Through a vibrating machine

**(a)** Mortar in which crushing the grains. **(b)** Sieving machine with sieves stacked.

**Figure 3.6:** Equipment for salt sieving.

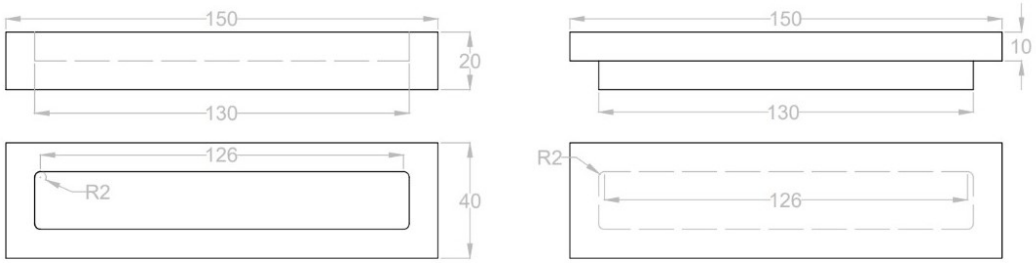


**Figure 3.7:** Project parameters of the moulds. Dimensions in mm.

(FILR.FTL-0150, Filtra vibración) the grains fell due to gravity. The time inside this machine varied from 30 minutes to 198 minutes, in a consecutive and fragmented manner (fig. 3.6).

Finally it was evaluated the possibility to dry the salt before being put in the machine heating it in a oven at 130°C for 30 minutes. After the heating, the salt was crushed again.

## 3.7 Creation of NaCl-PGS scaffolds

For the creation of this scaffold we based on the work of Vilariño-Feltrer et al. [39]. First of all we projected in Autocad® some moulds with the dimensions reported in fig. 3.7. We ordered them in Teflon® that resists high temperatures and does not stick to the polymer..

The moulds created combined different parameters such as the NaCl-pPGS ratio, the pressure with which the salt was crushed before pouring the prepolymer into it, the way to mix the salt and the prepolymer, the use of an high relative humidity environment (HR) and the use of nanosalt. With the exception of the experiment with the nanosalt, the salt used was a compound

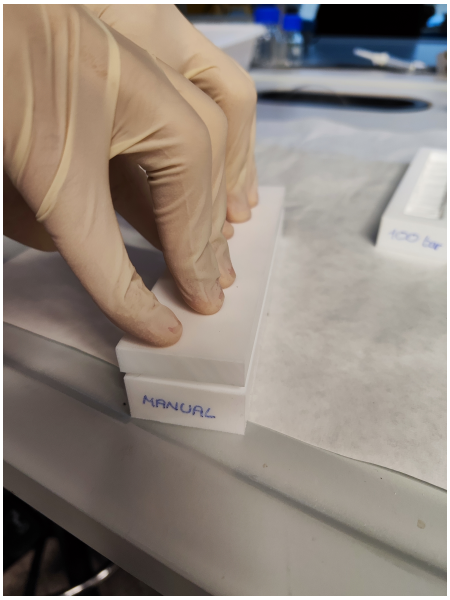


**(a)** Application of manual pressure only using hands and a spirit level.

**(b)** Use of a press to reach 100 and 200 Bar.

**Figure 3.8:** Pictures of different procedures for pressing and leveling the salt within the teflon moulds.

of 50% of 180-212 $\mu$m and 50% of 212-250 $\mu$m of grain diameter. Regardless of the conditions, the compound was treated for 48 hours at 130°C. In this way the cured PGS maintained the solid porous structure permanently.

### *3.7.1 Different pressure of compaction*

These experiments demanded four forces of pressure: zero, manual, that is crushing the salt with the lid of the mould manually, 100 Bar and 200 Bar. The last two pressures were obtained with an hydraulic press.

After smearing manually, with the help of a spirit level, we pressed the lid down with the palms of the hand. In the case without pressure, the lid was used only as salt leveller, in the the manual case we press with as much force as possible (fig. 3.8).

### *3.7.2 Different ways to mix the compound*

The mixture NaCl-pPGS was obtained in two different ways. In the first, the prepolymer was warmed in a oven for 10 minutes at 100°C, just to melt it, but without starting the curing process. Once dissolved, the mould was taken with the salt inside and it was caught trying to distribute it evenly on the surface. Then we put the mixture to cure and thanks to the low viscosity that has at high temperatures before curing, it infiltrated between the pores and the inlets of the grains of salt.

The second method always requires preheating the polymer to make it liquid, but unlike the previous one, the mixture is done manually, mixing, through a spatula, salt and pPGS on a Petri dish. Once a homogeneous mixture has been obtained, it is proceeded pouring it and distributing it in a homogeneous way on all the mould.

### *3.7.3 Different PGS-NaCl ratios*

Different material ratios can lead to different scaffold characteristics, such as the thickness of PGS walls, the percentage of porosity, the number of porous interconnections, resulting in changes in mechanical properties of the patch itself. For this reason, PGS-NaCl ratios were many. We tested the PGS:NaCl mass ratios 1:2, 1:3, 1:4, 1:5, 1:10, keeping the total volume constant, considering a patch height of 3 mm.

For the calculations of the respective masses these values were taken into account: volume of the patch $V = 130 \times 20 \times 3\,mm^3 = 7.8\,cm^3$, NaCl density $\delta_{NaCl} = 2.16\,g/cm^3$, prepolymer density $\delta_{pPGS} = 1\,g/cm^3$. The values are shown in the following table 3.1.

| **pPGS : NaCl ratio** | **pPGS fraction** [-] | **NaCl fraction**[-] | **pPGS mass** [g] | **NaCl mass** [g] | **Total mass** [g] |
|---|---|---|---|---|---|
| 1:2 | 0.333 | 0.667 | 4.61 | 9.22 | 13.83 |
| 1:3 | 0.250 | 0.750 | 3.65 | 10.94 | 14.59 |
| 1:4 | 0.200 | 0.800 | 3.01 | 12.03 | 15.04 |
| 1:5 | 0.167 | 0.833 | 2.56 | 12.78 | 15.34 |
| 1:10 | 0.091 | 0.909 | 1.46 | 14.57 | 16.03 |

**Table 3.1:** Mass of pPGS and NaCl for every mass ratio.

### *3.7.4 Nanosalt and relative humidity*

These last two methods have been used with the attempt to increase the size and number of connections between the pores generated by grains of salt. The idea is that using a percentage of salt grains with a diameter of the order of nanometers is necessary for them to settle between the contact points of the larger grains. This accumulation will increase the contact area between the grains and when the molten pPGS will creep around them, it will generate more intermediate holes.

For this type of scaffold not sieved salt was grinded with a mill (Retsch® ZM 200, fig. 3.9b), then we used a 20:40:40 of nanosalt:180-212:212-250 salt size ratio.

The use of salt stored in a humid environment serves to ensure that the grains in contact with them can melt, giving rise to an agglomeration with greater contact points.

A solution of distilled water and potassium sulphate (Sigma-Aldrich) was saturated and placed into a closed methacrylate chamber to achieve a relative humidity (HR) (fig. 3.9a) of 97% at 37°C in a oven (for reference, see the table 2 of Greenspan's work [40]). Then the salt, already in the mould was placed inside for at least 24 hours.

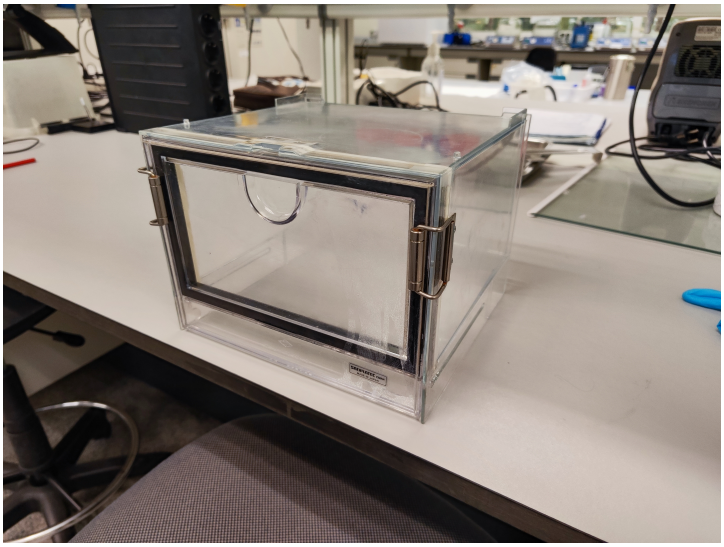

**(a)** Methacrylate chamber to reach an high humidity environment.


**(b)** Retsch® ZM 200, the mill to grind the salt into nanosalt.

**Figure 3.9:** Laboratory devices.

## 3.8 Salt removal from the scaffold

The removal of the salt from the scaffold, once cured the PGS scaffolds, to keep the polymer porous structure, took place by immersing the patch in milliQ water. Once extracted, they were immersed in 200 ml of milliQ ultra distilled water, containing a conductivity between 0.4-0.6 $\mu$S/cm. The patch was left to stand for days replacing the previous water with a new regular cycle, in the morning and afternoon, at 9.30 am and at 4.30 pm. Through a conductivity meter (Crison EC-Meter BASIC 30+, fig. 3.10), the conductivity of water was measured and changed until it reached a value similar to that of distilled water ($\approx$ 10 $\mu$S/cm). Containers with water and patch, were placed over a stirrer at 120 rpm.

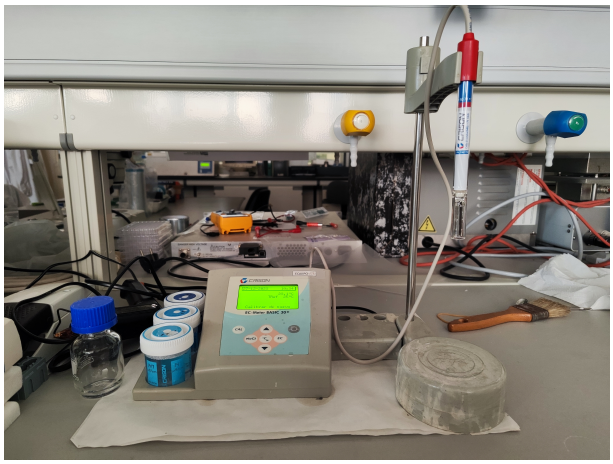

**Figure 3.10:** Conductivity meter setup.

**(a)** Cut of PGS patches **(b)** Deposition of the cut parts.

**Figure 3.11:** Processing steps for FESEM. Each test piece is formed by the cut on the left, corresponding to the lower face, and the one on the right corresponding to the upper one. The black tape under the test pieces represents the adhesive conducting tape.

The drying of the patches took place with an initial manual drying with filter paper being careful not to press too much to prevent the pores from collapsing. They were then left for 3 days under an vent hood, covered with filter paper, and dried again under vacuum for other two days.

## 3.9 Field Emission Scanning Electron Microscope (FESEM)

The objective of this phase is to evaluate qualitatively the arrangement, size and connection of the pores. First the patches were frozen with hydrogen to allow a clean cut of the sample with a razor blade (fig. 3.11a) avoiding to distort the holes. Each patch provided several samples for statistical analysis. They have been cut with rigour and order to easily distinguish the upper and lower sides of the cutting plane of each element. Once cut, they were placed on the sample holder with a conductive double-sided adhesive tape (fig. 3.11b). The external surfaces in contact with the Teflon mould and the water were also photographed to see how different they could be.

The next step is to cover the specimens with a conductive powder, to improve the resolution in the FESEM, carbon adhesive CCC (Electron Mycroscopy Sciences) was used as conductive coater, followed by a thin gold layer applied in the Leica EM MED020 (fig. 3.12a) under argon atmosphere.

Finally, the samples were analyzed with the ZEISS Gemini Ultra55 (fig. 3.12b) taking photos at both ends (top and bottom) with 100x zoom and one where the audition was shown in its entirety at 25x.

From the images obtained from the second group of samples, the average values of the pore size and interconnections were calculated through a software (Fiji®) that allowed us to find the area


**(a)** Leica EM MED020.

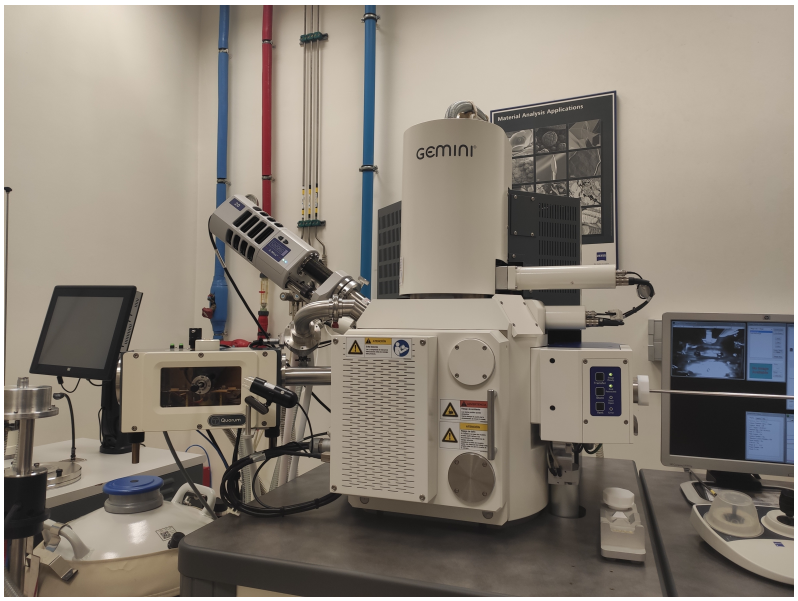


**(b)** ZEISS Gemini Ultra55.

**Figure 3.12:** Laboratory devices


**Figure 3.13:** Hydrostatic scale. The weight is placed in the submerged grid, while at the top the sample can be weighted before submerging it and then the weight can be calibrated

and the ratio of the diagonals of a hypothetical elliptical shape. To do this, the size of ten pores of every patch were taken into account, and 150 grains of salt, 50 for every grain size (180-212, 212-250, nanosal) were measured.

## 3.10 Porosity calculation of porous patch

The formula used to measure the porosity $\pi$ of a material is:

$$\begin{aligned} \pi &= \frac{V_p}{V_{tot}} \\ &= \frac{m_{H_2O}/\rho_{H_2O}}{V_s + V_p} \\ &= \frac{m_{H_2O}/\rho_{H_2O}}{m_s/\rho_s + m_{H_2O}/\rho_{H2O}} \end{aligned} \tag{3.1}$$

where $V_p$ is the pore volume, identified as the ratio between the mass and the density of the fluid inside them ($m_{H_2O}$, $\rho_{H_2O}$), in this case water. $V_{tot}$ is the total volume composed by the sum of the sample volume $V_s$ and the pore one; $m_s$ and $\rho_s$ are respectively the mass and the density of the sample.

The mass of the patch and that of the water were easily obtained with a balance going to weigh the sample dry, then filled with distilled water and finally making the difference between the masses. To make sure that all the pores contained water and that the air was all expelled, the patch was inserted inside a syringe filled with fluid. At that point the vacuum was generated going to clog the nozzle and pulling the piston, until the air bubbles can be seen coming out. The process has been repeated several times.

The density of water can be obtained from tables by measuring only the reference temperature, while that of the specimen requires a hydrostatic balance (fig. 3.13). It allows to measure the

mass of the fluid displaced following the principle of Archimedes that states that a body immersed in a fluid receives a push from the bottom upwards equal to the weight of liquid displaced. We know in fact that the weight measured by the balance is nothing more than the difference between the weight of the object and the weight of the fluid, therefore going to subtract from this result the weight of the object not immersed can bring to get the weight of the fluid, which divided by $g$ provides the mass of the liquid $m_w$. The volume of water moved is equal to the volume of the dry patch, accordingly:

$$\begin{aligned} V_p &= V_w \\ V_p &= \frac{m_w}{\rho_w} \end{aligned} \tag{3.2}$$

Whereas the density of the patch is:

$$\rho_s = \rho_w \cdot \frac{m_s}{m_w} \tag{3.3}$$

Alternatively, the total volume can be calculated without calculating the density using the same method by calibrating the patch already filled with water.

## 3.11 Hydrogel production

### *3.11.1 HA hydrogel production*

The production of a scaffold based on hyaluronic acid is a long process that requires several days of preparation and considerable precision with the compounds. The chemical route is called "EDC/NHS chemistry" and it can be done in water and in room temperature conditions. The protocol followed is found in Bian *et al.* [41].

This hydrogel has been designed with a density ratio of 0.5% of weight/volume (w/v) [g/L]. 50 mg of hyaluronic acid (Sigma-Aldrich) were weighted with an analytical balance (Mettler-Toledo AX205) (fig.3.14a) and placed in a vial with 10 mL of milliQ water. This solution was then left to stand overnight in a freezer at 4°C with a rotating magnet inside.

The next day, 28.7 mg of NHS (N-Hydroxysuccinimide 98%, Sigma-Aldrich) were weighed in an fume hood and poured into the dissolution of HA, prepared the day before, and left to agitate for 10 minutes. Sonication was used to remove the air bubbles formed during agitation.

Inside the vent hood, 95.6 mg of EDC-HCl (N-(3-(Dimethylaminopropyl)- N - ethylcarbodiimide hydrochloride) (Sigma-Aldrich) and were thrown into dissolution. The compound of HA, NHS and EDC-HCl was then stirred for two hours at room temperature.

We proceeded with the addition of CSA·HCl solution (Cysteamine hydrochloride) (Sigma-Aldrich), a very hygroscopic compound requiring handling in a methacrylate chamber (fig. 3.14b) operating with nitrogen flow. Inside the closed cabin was placed a quantity of 427.36 mg of CSA·HCl inside a centrifuge tube (eppendorf, as it will be called from now on), to weigh it place approximate quantities in the cabin and then weigh with on the balance after closing the eppendorf, and then 1 ml of distilled water was added. We got a solution of 427.36 mg/mL of concentration.

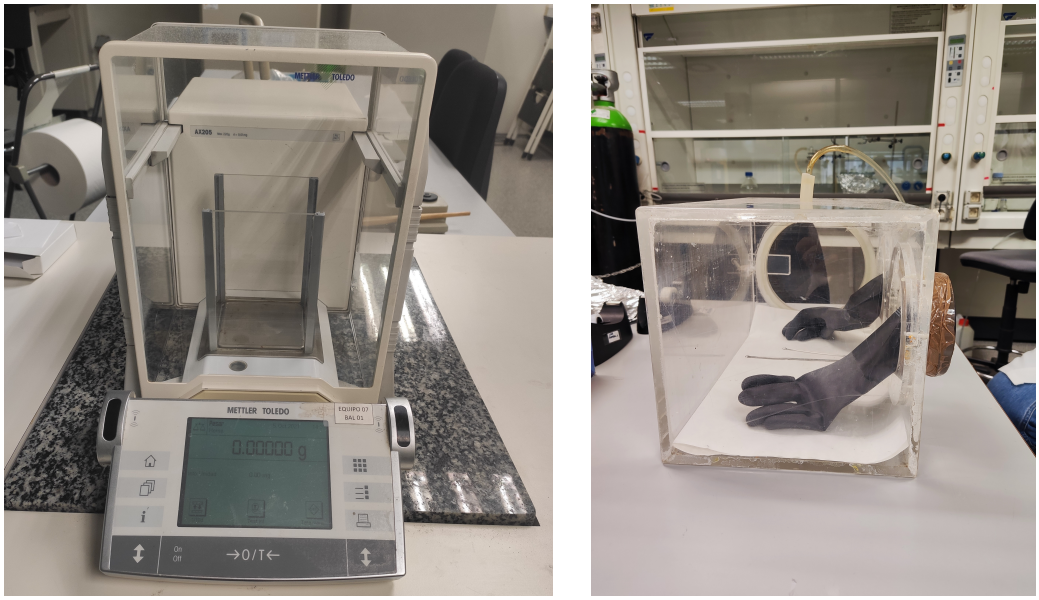


**(a)** Analytic scale Mettler-Toledo AX205 **(b)** Methacrylate chamber

**Figure 3.14:** Laboratory devices.

After two hours of shaking the EDC·HCl, 137 ml of CSA·HCl solution were added, corresponding to 58.42 mg of CSA·HCl. The pH was adjusted to reach the value of 4.75 with HCl and then left to agitate for 24 hours. This procedure, based in the so-called "EDC/NHS chemistry", allows the primary amine of the CSA to substitute the NHS that is attached to the -COOH of the HA, after activation by the EDC. This way, the -SH of the CSA is revealed as a functional group and, therefore, disulfide bonds cand crosslink the HA chains under certain conditions

The next day the solution was placed on dialysis and to do this it was necessary to hydrate the membrane (Spectra/Por3 Dialysis Membranes (MWCO: 3.5 kd)) for one hour in distilled water. Once hydrated the dissolution was posed in a buffer (100mM NaCl pH 3,5), one litre, because the amount needed is a thousand times the volume of dissolution inside the membrane for 24 hours.

The buffer and dissolution container was covered with aluminium to prevent the degradation of HA by light. It was then agitated for 24 hours.

The next day was the second dialysis, always for 24 hours, but with distilled water, to prevent the acidic biodegradation of the hydrogel. The result was evaluated with Ellman's Assay Protocol [42].


**Figure 3.15:** TMA/SS6000 (SII Seiko Instrument Inc.)

### *3.11.2 Production of PVA hydrogel*

The first step in making a PVA (Sigma-Aldrich) hydrogel is to create a 4% solution of PVA in distilled water. 4 grams of poly(vinyl alcohol) were dissolved in 100 ml of distilled water and left for 24 hours in reflux heating at 90°C in oil, to dissolve over the Tg of PVA (around 85 ºC), to boost the speed at which it can be dissolved. In the meantime, the cross-linking agent was prepared by placing 1 gram of sodium tetraborate (Sigma-Aldrich) in 4% solution in 25 ml of distilled water and then mixing them.

## 3.12 Thermomechanical Analysis

Mechanical tests consisted of temperature-controlled compression tests, i.e., thermomechanical analysis (TMA). The objectives of these tests were to obtain a stress-strain graph at 37 °C to simulate the behaviour of the patch in contact with the skin.

The samples to be compressed were cut from PGS patches to form cylinders 3 mm high and 8 mm of diameter-cylinder. From each patch eight samples were extracted. Four of them were refilled with distilled water with the method described in sec. 3.10, while the others with the PVA solution and then immersed for 30 minutes in the solution of sodium tetraborate. 3 mm thick discs of cured PGS with and without 1 mm thick PVA hydrogel layer were used as control.

The compression rate was 10 mN/min for ten minutes. The TMA machine used was TMA/SS6000 (SII Seiko Instrument Inc.) in fig 3.15.

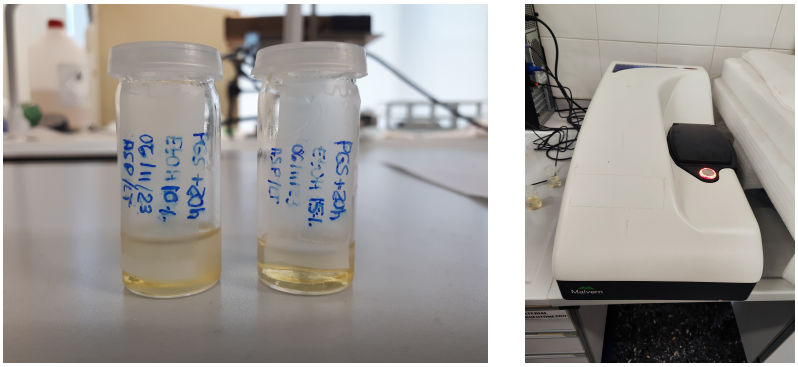

**(a)** Example of solution test. Below a part of undissolved polymer can be seen.

**(b)** Zetasizer Nano Z590

**Figure 3.16:** In the left the PGS:ethanol solution, that will be analysed with Zetasizer, in the right.

## 3.13 Procedure for the electrospun membrane solution

The idea is a solution that must be composed of PGS as cured as possible, but such that it can be soluble with a solvent for PGS, ethanol. The prepolymer of PGS was put in vials to reach 1 mm of height when melted. The hours of curing varied from 10 to 30 hours. Then ethanol was added in every vial to get a % m/v [mg/ml] varying from 10% to 75%. Each vial was left in agitation for several days to assess the dilution time of the PGS. Once dissolved, the supernatant part was removed and stored to be use for electrospinning, whereas the remaining part was weighed to calculate the percentage of dissolved material.

## 3.14 Dynamic Light Scattering

Dynamic Light Scattering (DLS) is a technique used to measure the particle size in a liquid solution. By analysing fluctuations in scattered light intensity over time, DLS captures the random Brownian motion of particles, providing valuable insights into particle size distribution. The measurement of the zeta potential is performed by assessing the speed at which particles move in response to an electric field. It was used to evaluate the curing grade of PGS in the ethanol solution because at some point, during the PGS synthesis, the hyperbranched macromolecules formed are though to be big enough, yet soluble, to be detected at the nanometre range. Zetasizer Nano Z590 was utilized (fig. 3.16). The dispersant was ethanol at 20°C, viscosity 1074 mPA·s, RI 1361, equilibration time 120 seconds, measurement angle 90°, number of measurements 3, delay between measurements 10 seconds, numbers of run 11, run duration 10 seconds.

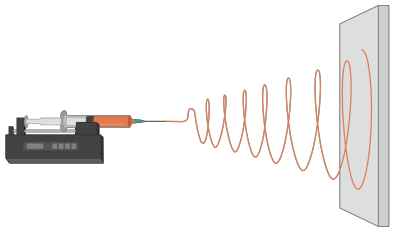

**Figure 3.17:** Example of operation of electrospinning. A polymer fibre exits a nozzle and reaches the collector with a random arrangement by means of a high electric field.

## 3.15 Electrospinning

Electrospinning is a sophisticated nanofabrication technique utilized for the creation of nanofibers from a diverse range of materials. Widely applied in fields such as materials science, biotechnology, and medicine, this process stands out for its ability to produce ultrafine fibers with diameters ranging from a few nanometers to several micrometers.

In practice, a polymer solution is meticulously prepared by dissolving a selected polymer in a suitable solvent. This solution is then loaded into a syringe equipped with a metallic needle, known as a spinneret, which is connected to a high-voltage power supply (fig. 3.17).

As the high electric field is applied between the spinneret and a grounded collector, it induces a charge on the droplet of polymer solution at the tip of the spinneret. This electrostatic repulsion forces overcome the surface tension of the polymer solution, resulting in the formation of a fluid jet.

During the journey of the jet towards the collector, solvent evaporation occurs, causing the polymer to solidify and form nanofibers. The arrangement of the collector determines the alignment and morphology of the fibres. The resulting nanofibres are collected on the grounded collector, forming a nonwoven matrix or membrane.

The characteristics of the membrane obtained through electrospinning depend on various factors that can be managed during the process. Process parameters, such as electric voltage, feed rate, and the distance between the spinneret and collector, significantly impact the formation and growth rate of fibres. The composition of the polymer solution, including the type and concentration of the polymer, influences the chemical and physical properties of the resulting membrane.

The addition of auxiliary agents like cross-linking or functionalising agents can modulate the structure and performance of the membrane. Environmental conditions, such as humidity and temperature, and collector features further contribute to fibres formation and membrane morphology.

Additionally, properties of the polymer itself, such as molecular weight, play a role in fibre formation.

In our case we played with the distance between spinneret-collector changing it between 15 and 25 cm. We used the most accurate and simultaneously more concentrated ethanol solutions - prepolymer starting from the sample of 19h and 25 % to the more concentrated of 22h and 75 %. Outside temperature was around 22°C, while inside the insulating chamber was around 23 °C. Humidity was 32% and 23% respectively. The chosen voltage was 10-25 kV, while the ejection rate of the syringe containing the solution varied between 0.5 ml/h and 1 ml/h. It had a volume of 12 ml, while the diameter of the needle was 16.6 $\mu$m. The rotating collector turned at 13 rpm.

## 3.16 Statistic tests

All the tests were done with the software GraphPad® Prism. To measure the normality of a distribution, the Shapiro-Wilk test was used. Two-way Anova test and multiple comparisons of Tukey were used to compare normal data, while Mann-Whitney U test and Kruskal-Willis not parametric tests were use to analyse not normal data. In all the tests it was considered statistically significant p-value of $< 0.05$.

# Chapter 4

# RESULTS AND DISCUSSION

## 4.1 Reproducibility of the PGS production process

Given the many variables that can affect the PGS production process, this experiment was intended to observe the reproducibility of the polymer cure, which was produced in five specimens, four under the same conditions in vials and a sample called M1 that was produced in the Teflon mould. All were produced as 1 mm PGS layers. It was evaluated by observing the fusion peak temperature in a DSC test and by the ratio of functional groups in an FTIR test. The samples were called M1, M2, M3, M4, M5.

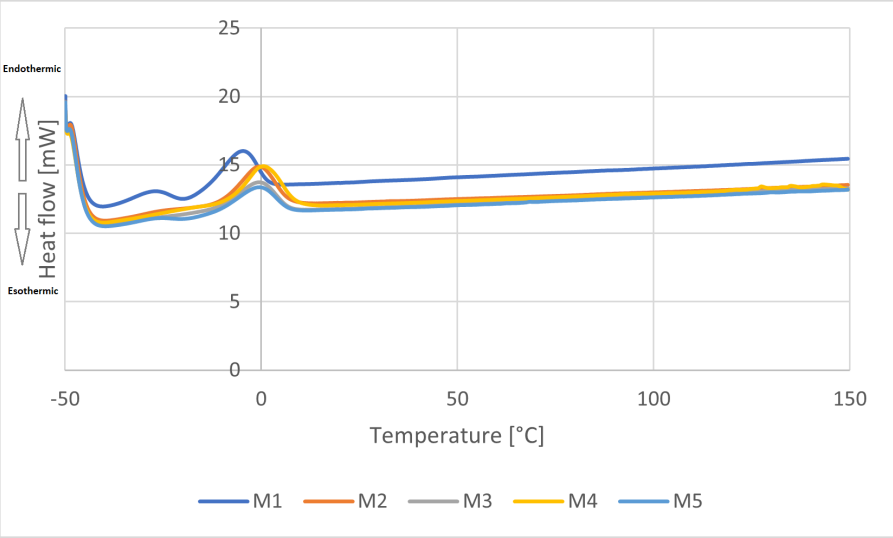


**Figure 4.1:** DSC reproducibility test of the 5 specimens.

The fusion temperatures were easily found because for PGS it has the shape of an upward peak, since it is an endothermal process. The temperatures found in fig. 4.1 were:

| | M1 | M2 | M3 | M4 | M5 |
|---|---|---|---|---|---|
| T [°C] | −4.82 | −0.69 | −0.73 | 0.47 | −0.96 |

**Table 4.1:** Fusion peak temperature of the samples.

The results in table 4.1 shows that samples produced with the same conditions, M2-M5, have almost the same fusion temperature, whereas M1, that differs only for the mould, has a different temperature. The standard deviation is very low, since it is 2.02°C considering the 5 samples and just 0.64°C with only M2-M5. Calculating the coefficient of variation (the full scale is −50 - 150°C) this represents 1.01% or 0.32% respectively, i.e. a really low variation between samples.

FTIR results are shown in fig. 4.2:

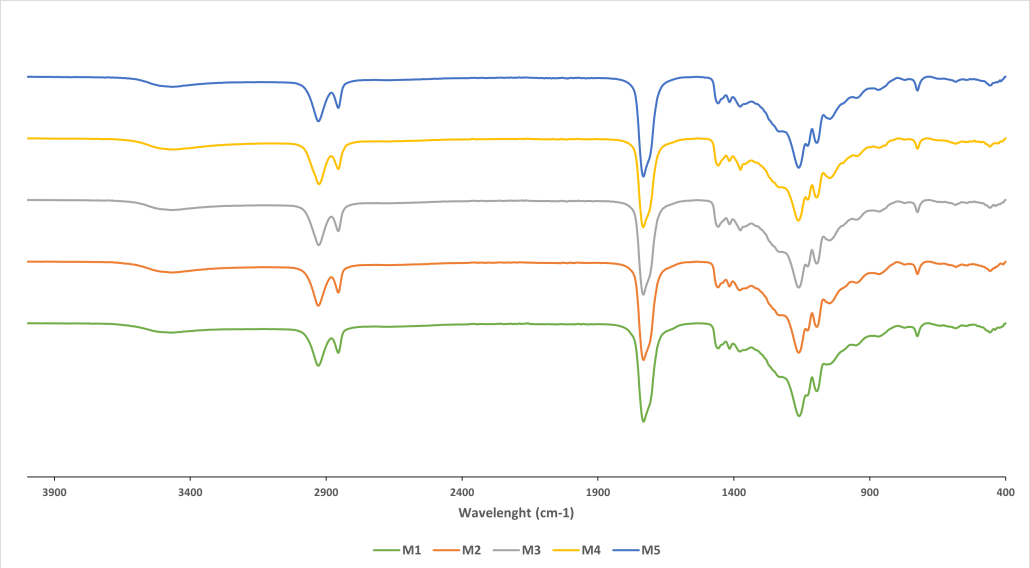


**Figure 4.2:** FTIR results of M1-M5 samples.

The peaks of the hydroxyl, esters and carboxyl groups are found at wavelengths 3200-3600 (green), 1720-1740 (red), and 1690-1710 (blue) $cm^{-1}$ respectively (tab. 4.2):

| | M1 | M2 | M3 | M4 | M5 |
|---|---|---|---|---|---|
| Hydroxyl | 93.86 | 92.80 | 93.41 | 92.71 | 93.39 |
| Ester | 36.06 | 35.95 | 38.42 | 42.28 | 35.18 |
| Carboxyl | 47.58 | 47.40 | 50.91 | 54.06 | 47.99 |

**Table 4.2:** Hydroxyl, ester and carboxyl group transmittance peak of every sample.

and the hydroxyl/carboxyl and the hydroxyl/ester ratio are (tab. 4.3):

| | **M1** | **M2** | **M3** | **M4** | **M5** | **Mean** | **SD** |
|---|---|---|---|---|---|---|---|
| -OH/-COOH | 1.97 | 1.95 | 1.83 | 1.71 | 1.94 | 1.88 | 0.09 |
| -OH/-COOR | 2.60 | 2.58 | 2.43 | 2.19 | 2.65 | 2.49 | 0.16 |

**Table 4.3:** Hydroxyl/carboxyl and hydroxyl/ester ratio of every sample.

This ratios, that gives a qualitative idea of the curing grade, do not show a substantial difference between them.

FTIR and DSC analysis show that under the same curing conditions, PGS provides an elastomer with the same properties and differences are negligible for all M1-M5, but we wanted to study further the effect of changing slightly the shape or the depth of the mould, since this would have a great impact in the design of the moulds and cuvettes for PGS films and scaffold preparation.

## 4.2 PGS curing in confined volume

The reaction that leads to the production of PGS is a condensation reaction. The removal of water is very important because its possible remaining between the chains of the polymer would block the progress of the reaction itself. During the curing process, the polymer is put at 130°C and the water is removed by evaporation. However, if the surface from where it can evaporate is small, the viscosity of the polymer, especially during the curing, will hinder mass transfer of the water through the reaction mixture, slowing the process.

The objective of this experiment is to assess the degree of curing by observing how close it is to the melting temperature peak of the treated PGS or prepolymer. For this experiment an 8 cm high vertical mould was used with a narrow 2 mm slits. After treatment for 48 hours, samples were taken at 5 different heights, in all cases they all had Teflon under them, so that they would not be affected by evaporation of polymer mixture under them, fig 4.3. The top to bottom samples were named D1, D2, D3, D4, D5, respectively.

The peak temperature of each is (tab. 4.4):

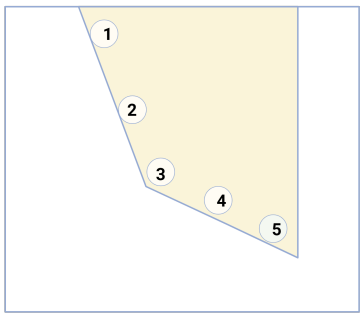


**Figure 4.3:** Scheme of samples taken at different heights from the vertical mould.

| | PGS+48 | D1 | D2 | D3 | D4 | D5 | pPGS |
|---|---|---|---|---|---|---|---|
| T [°C] | −12.01 | 7.27 | 7.44 | 7.33 | 8.48 | 8.69 | 11.09 |

**Table 4.4:** Fusion peak temperature of the samples

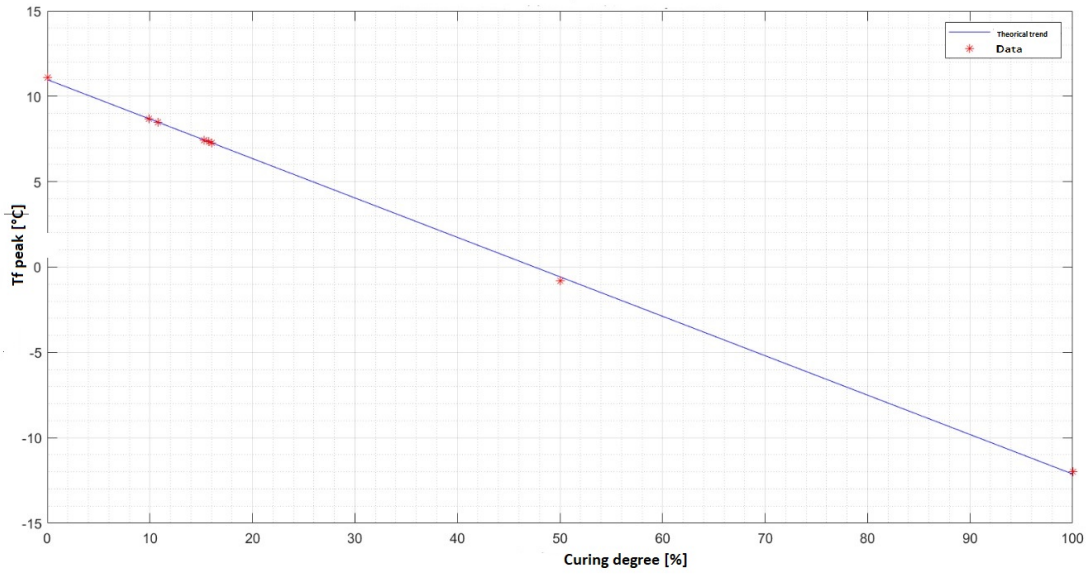


**Figure 4.4:** Theoretical trend of fusion peak depending on the curing time. Here pPGS peak is supposed to be 0% and the 48h cured PGS one 100%.

These values indicate that every sample is much closer at the curing grade of the pPGS, supposed zero, than the cured PGS one, supposed 100, fig.4.4. It can be noted that the first 3 have close values, as well as the last two. Looking at the image 4.3, we notice that the first three, in addition to being closer to the surface, are adjacent to a more inclined wall. This may encourage the escape of water that encounters less tension by passing between the wall and the polymer, rather than passing through the polymer. The values do not differ a lot between them, and represent a poorly cured PGS (10-20 % cured) even if they were at 130°C for 48 h.

The next step was to use the same production process, but increasing the curing hours to 72. The result was this in fig. 4.5:

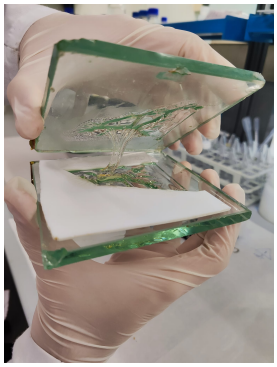

**Figure 4.5:** Cured PGS in confined volume 72 hours.

From the image it is clear that by increasing the treatment time by 50%, a rather viscous dough is obtained, far from the goal of obtaining an elastomer. We opted to change strategy, removing most of the water molecules before the cross-linking process. It was decided to freeze-dry the prepolymer as more efficient method than evaporation. What was obtained was a polymer visibly not cured, but that at room temperature was solid and not liquid like the previous one.

Then we analysed five sample in the same order of the previous one to check the fusion peaks. These temperature were (tab. 4.5):

| | **F1** | **F2** | **F3** | **F4** | **F5** |
|---|---|---|---|---|---|
| T [°C] | 6.85 | 6.23 | 6.33 | 5.64 | * |

**Table 4.5:** Fusion peak temperature of the freeze-dried samples. F5 was not analysed for technical problems.

Comparing the data with those of the first experiment, we can see that the trend is the same, with more accurate areas on the surface and close to inclined walls. It is also clear that by freeze-drying the crosslinking is improved. But we cannot be satisfied with the degree of curing because the values are far from a theoretical −12°C. Further studies could be done by greatly increasing the hours of treatment or studying the area/depth ratio, but from a practical point of view it is evident the difficulty to cure under these conditions. This result influenced the design of the moulds of the following experiments, i.e. with a great surface in contact with air and a low depth.

## 4.3 Porous scaffold creation

### *4.3.1 NaCl sieving*

NaCl is the salt used to create porous scaffolds combined with PGS polymer. The scaffolds, however, can not contain pores too large or abundant because the structure could be too fragile. At the same time too small or too few pores make it very difficult to insert the hydrogel into the patch. The salt used for this experiment contained grains of varying sizes ranging from tens of micrometers to several hundred in diameter. We needed specific ranges, namely 180-212 $\mu$m and 212-250 $\mu$m. Because of the large quantities needed to produce the patches and the required accuracy, we needed a reliable and reproducible sieving method.

We used sieves of decreasing diameter piled on a vibrating machine. The first thing we analysed is the amount of salt placed. Quantities ranging between 100 g (fig. 4.6a) and 10 g (fig. 4.6b) were sieved for 200 minutes and compared. From the graph it was noted that in the 100 g salt sample it did not go down from the sieve of 150 $\mu$m, while passing in the 10g one. We assumed that a large amount of NaCl blocked the process because it clogged the pores by not letting pass the smaller grains that would pass through.

We started measuring bigger and bigger quantities to find a limit point where the pores were clogged, but that did not change, so we thought the problem was related with humidity. It bound the grains together and the shock of the vibrations was not enough to separate them and let them pass. 50 g of salt was then heated 30 minutes to 130 °C before being sifted (fig. 4.6c). The graph shows how all the grains could pass without obstacles to the last sieve.

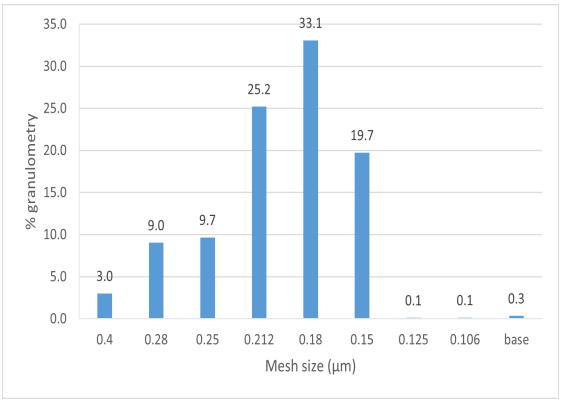


**(a)** 100 g not heated.

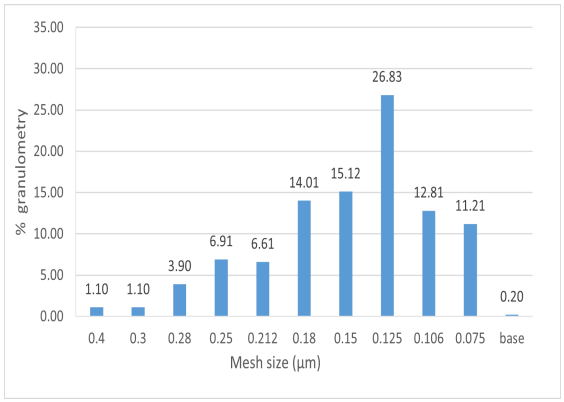


**(b)** 10 g not heated.

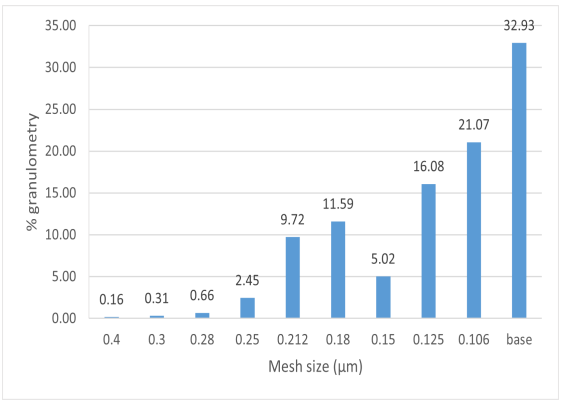


**(c)** 50 g heated.

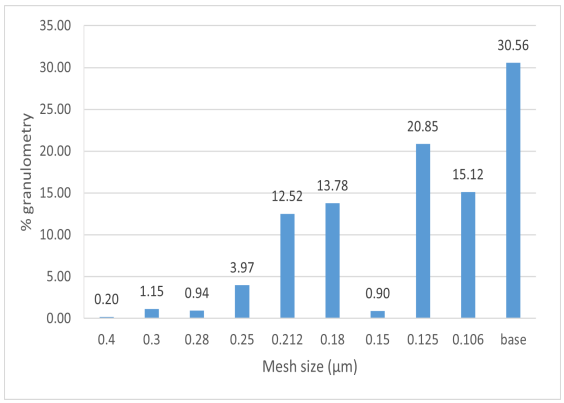


**(d)** 100 g heated.

**Figure 4.6:** Histograms on the percentage of mass deposited on each sieve after each sieving.

Finally, we moved on to the optimization process, reducing the time up to 30 minutes of sifting and sifting 100 g at a time (fig. 4.6d).

### *4.3.2 NaCl removing time from porous scaffolds*

This part was necessary to understand the time it took to remove salt from the porous scaffold. The process took place between the creation of the scaffold and the study of electron microscopy with FESEM, explained in section 4.3.3. After each wash, the conductivity of the water samples with NaCl dissolved was measured. The objective was to obtain a conductivity similar to that of distilled water of about 10 $\mu$s/cm. From the figures we observe that the HR specimens have reached the objective conductivity in only 48 hours, while the Nano specimens are the ones that have taken longer, more than 160 hours. CP took 96 hours, no distinction between mass ratio. Finally M and SP took two different times depending on the ratio. What is clear from figure 4.8 and 4.7 is that the time of each technique differs, in particular the ratio 1:4 is faster because of the size of the pores that facilitates the passage of salt. On the contrary, Nano has the longest times for the same reason.

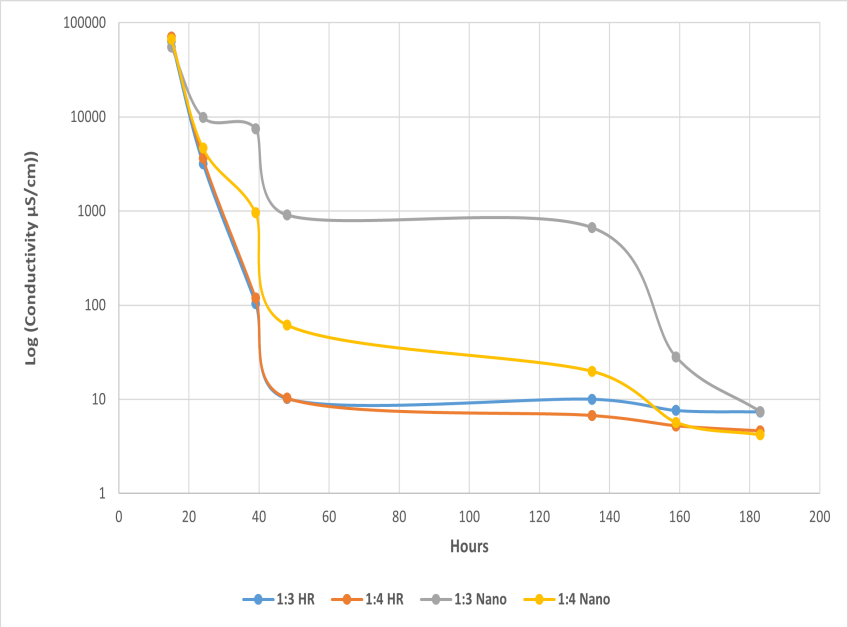


**Figure 4.7:** Conductivity of the water with which NaCl was dissolved and removed from the scaffold after each wash, as a function of the hour from the first wash. HR = relative humidity, Nano = Nanosalt, 1:3 1:4 = PGS:NaCl ratio.

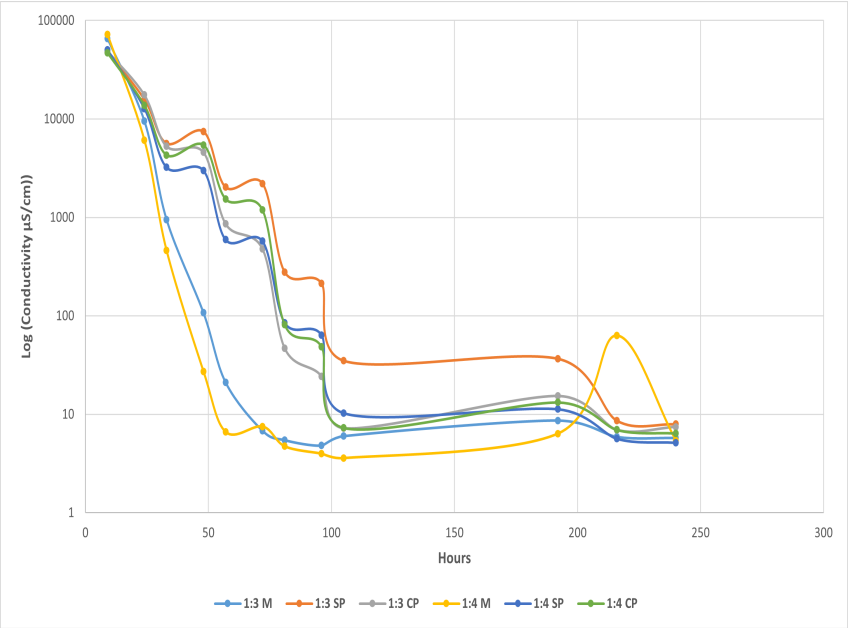


**Figure 4.8:** Conductivity of the water with which NaCl was dissolved and removed from the scaffold after each wash, as a function of the hour from the first wash. M = mix, SP = without pressure, CP = with pressure, 1:3 1:4 = PGS:NaCl ratio.

### *4.3.3 Evaluation of the porous scaffolds through FESEM*

First, several preliminary scaffolds were made to evaluate the best PGS:NaCl ratio and different techniques of salt compaction before pouring the polymer into it. Manual pressure was applied by pressing the mould cap against the salt inserted inside. The pressures at 100 Bar and 200

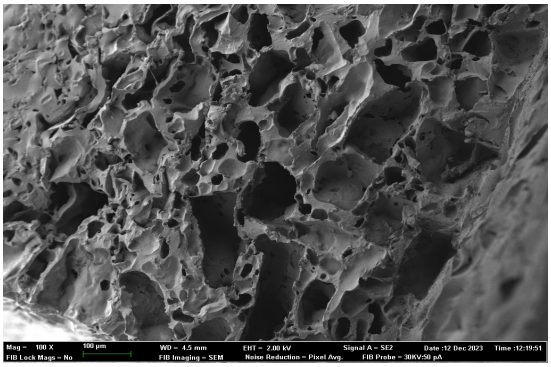

**(a)** 100 Bar.

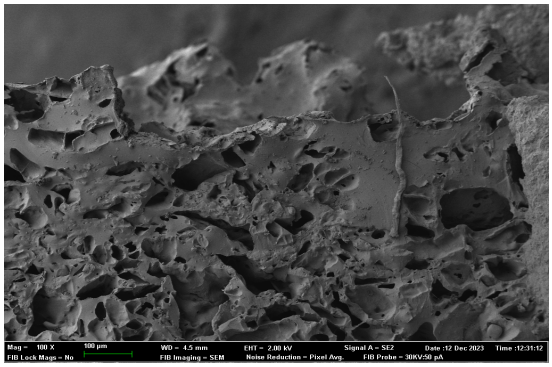

**(b)** 200 Bar.

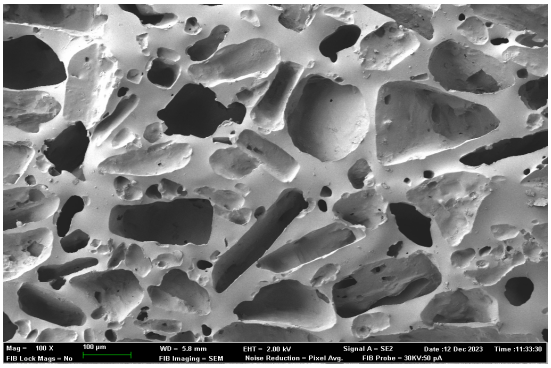

**(c)** 1:2 ratio.

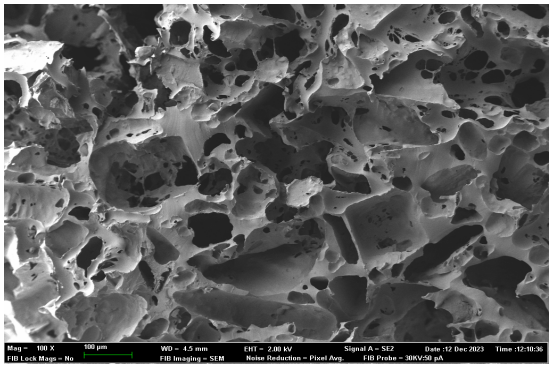

**(d)** 1:3 ratio.

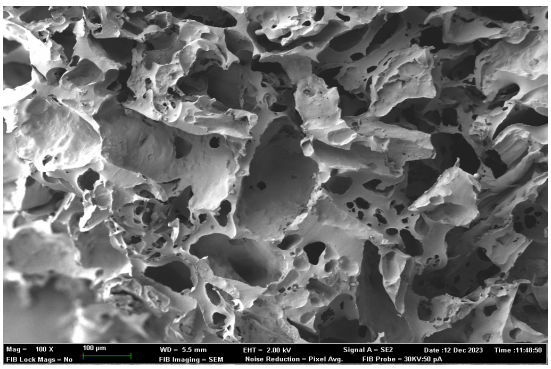

**(e)** 1:5 ratio.

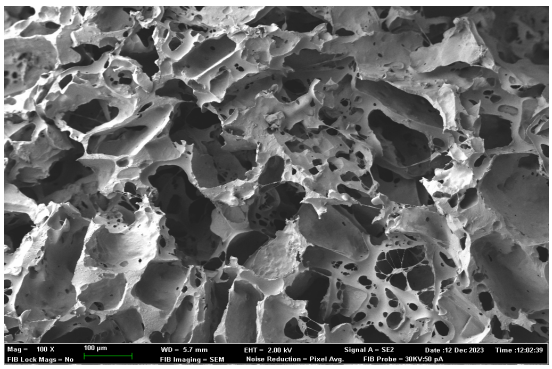

**(f)** 1:10 ratio.

**Figure 4.9:** FESEM analysis of the sample with manual, 100Bar, 200 Bar pressure and 1:2, 1:3, 1:5 and 1:10 PGS:NaCl mass ratio. Pressure test were done with 1:3 mass ratio. Scale bar = 100 $\mu$m.

Bar were done through a hydraulic press. A preliminary analysis showed that too high pressures deformed the mould making it unusable (fig. 4.10). After every curing, the salt was removed by solution in milliQ water. Exhibition 1:10 was clearly unacceptable as a scaffold, since it was broken up into several pieces during washing.

The analysis at FESEM confirmed that the samples obtained by hydraulic press were distorted and crushed with few interconnections and very tight pores, figs. 4.9a, 4.9b. As for her ratios 1:2, 1:3, 1:5 and 1:10, it was immediately apparent to the eye that 1:10 had too many pores and poorly connected, making a hypothetical structure too fragile (fig. 4.9f). In contrast, 1:2 had too few interconnections between pores, making them isolated and non-communicating (fig.

**Figure 4.10:** Cured PGS in confined volume 72 hours.

4.9c). All these options have been discarded. 1:3 and 1:5 seemed appropriate since 1:3 had more interconnections, the ratio 1:3 and 1:4 were further studied (fig. 4.9d). As for the pore size, it was not measured on the FESEM pictures, since it would have implied an image analysis of low consistency because of the view depth, ad these pores were strictly in the same range of the original salt (fig. 4.11).

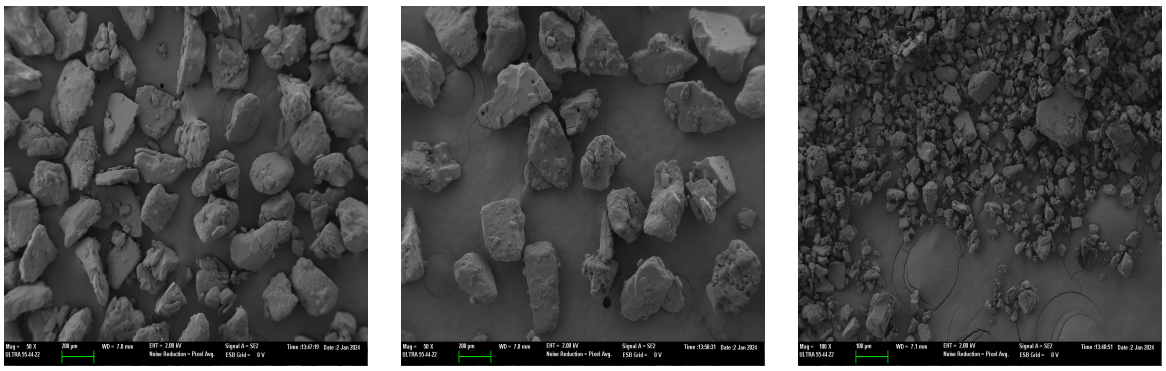

**(a)** 180-212 $\mu$m. **(b)** 212-250 $\mu$m. **(c)** Nanosalt.

**Figure 4.11:** FESEM images of the grain dimension: 180-212, 212-250 $\mu$m and nanosalt. Scale bar = 200 $\mu$m for (a),(b); 100 $\mu$m for nanosalt.

The second part of the evaluation compared the ratios 1:3 and 1:4 with different mixing techniques. Each ratio has been studied by mixing manually molten PGS and salt (M), PGS poured on compacted salt (CP) and PGS poured on uncompacted salt (SP). The addition of a percentage of salt with a diameter in the order of nanometers (Nano) and the use of a high humidity chamber where salt is placed (HR) were also tested. The latter two have served to study a possible increase in the interconnections between grains. The moisture would melt the grain contact point between grains, the nanosalt would infiltrate the contact points and create free volume.

Of these samples, the areas in contact with the outside and the internal parts were analysed with electron microscopy. The micrographs on the external surfaces showed that some samples showed flat surfaces without pores in the areas in contact with the Teflon mould. This implies that a hypothetical future patch will hinder release bioactive substances in that direction. About these samples, only 1:4 M seemed not to have a flat contact with the mould (fig. 4.12)

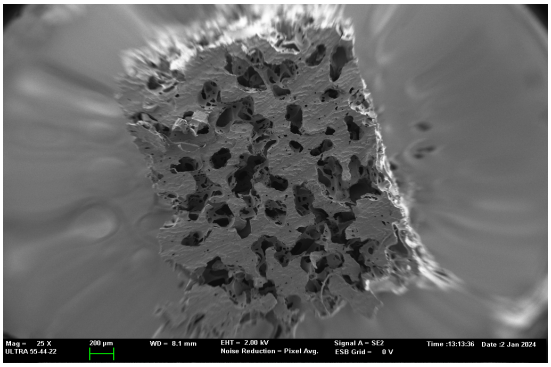

**(a)** 1:4 SP external surface.

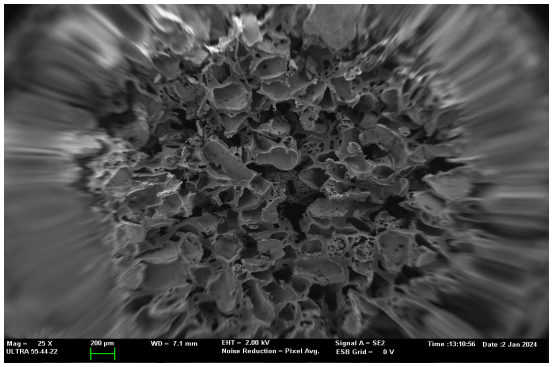

**(b)** 1:4 M external surface.

**Figure 4.12:** FESEM analysis of the external surface in contact with the mould of the sample 1:4 SP and 1:4 M. Except for the right one, all had the same shape of 1:4 SP. Scale bar = 200 $\mu$m.

The internal structure has been evaluated by means of the average of the axis length of a hypothetical ellipsoid shape, as reference of the interconnections found between pores. The important factor is the minor axis that provides the minimum size for which biomolecules can pass through the pores.

To make a statistical analysis, each sample of each patch was photographed at three points near the surface in contact with Teflon (bottom) and at three points in the opposite direction (top). The first thing we did was an analysis to test the normality of axis data, which was negative. Subsequently, the Mann-Whitney U-not parametric median comparison test was used to verify that there were no discrepancies between top and bottom, and the data was found to be related, fig. 4.13. Finally, they were compared using the non-parametric Kruskal-Willis test, which compares the medians with a 95% confidence interval. The results of this test (fig. 4.14) give us only some appreciable results. In fact, we can see that the lower median axis of each group is a few tens of $\mu$m, which is exactly the minimum size required for the Therapatch project. However, this data does not provide information on the number of interconnects, which is of fundamental importance, because it is still possible that a patch has the size of the appropriate interconnections, but they are insufficient to connect the pores well. Observing the values suggested by the graph, it is not clear whether a 1:3 ratio is better than a 1:4 ratio. However, it can be noticed that the data with a smaller minor axis are 1:3 SP, 1:4 CP, and 1:3 HR, while the best is 1:3 Nano. The M technique is the only one where the values are high regardless of the mass ratio.

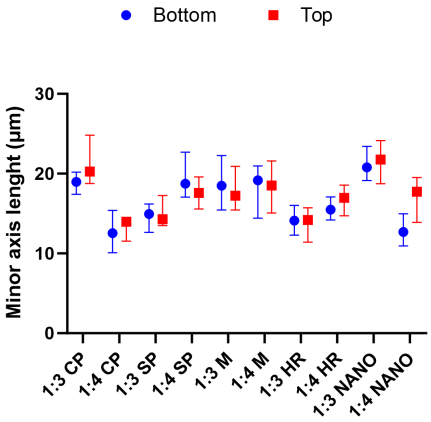


**Figure 4.13:** Mann-Whitney U - not parametric median comparison test between top and bottom minor axis length, $p < 0.05$. Red squares represent the top axis, blue circles the bottom axis.

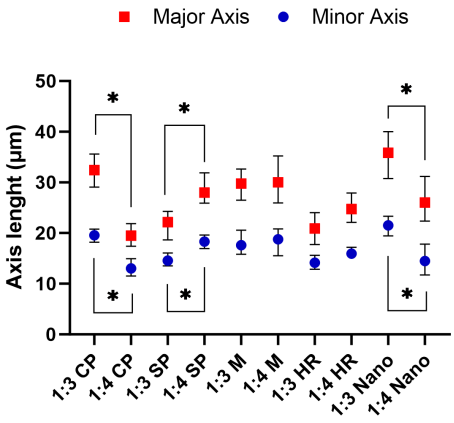


**Figure 4.14:** Kruskal-Willis test of the minor and major axis of the interconnections between pores, $p<0.05$. Red squares represent the major axis, blue circles the minor. Points show the median with 95% C.I.

### *4.3.4 Handling of the creation techniques*

Among the techniques studied during the second phase explained in the paragraph 4.3.3, SP and CP have been used in combination with the pouring technique. When the scaffold was removed from the mould, it was found that the polymer did not distribute well in all areas and scaffolds with irregular shape and thickness were obtained. Mixing PGS and salt with the spatula guarantees a homogeneous distribution. Both nanosalt and HR distributed well, the first mixing, the second pouring, however HR took an extra day to prepare to allow the salt grains to humidify. The difference of the mixing/pouring technique can be observed here too, even if in a minor way, fig. 4.15. Another factor concerns the handling of the scaffolds. All of them were easily removable from the moulds, except for those using the pouring technique, which turned out to be sticky, forcing us to damage them with a spatula to remove them.

**(a)** SP patch, obtained with pouring technique.

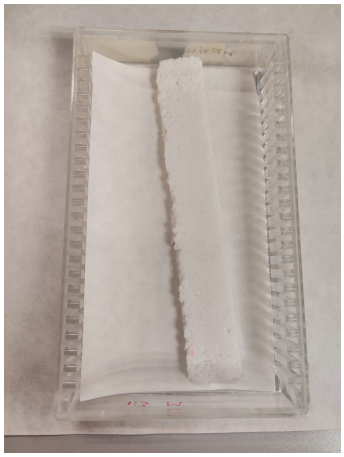

**(b)** M patch, with mixing technique.

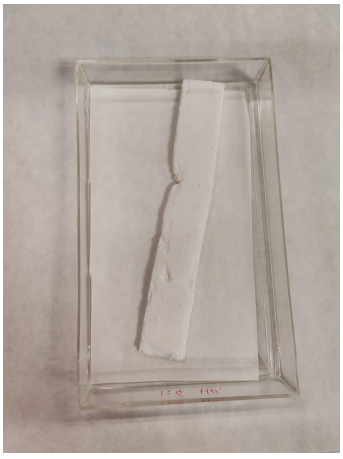

**(c)** HR patch, obtained with pouring technique.

**(d)** Nano patch, with mixing technique.

**Figure 4.15:** Porous patch after being cured and the removal of the salt.

### *4.3.5 Porosity of the scaffold*

The porosity of the specimens has a lot of weight for the choice of the preferred technique. First, the CP and SP specimens show the lowest porosity of all, all below 60% regardless of the proportion used. In all other techniques, the porosity is higher and the difference between 1:3 and 1:4 is noted in M and Nano, the former being greater. Very interesting is the case 1:4 M with a porosity of more than 75% and the smallest standard deviation, the best (results in fig. 4.16). The test was done with two-way Anova test with a Tukey test for multiple mean comparison, with significant differences at $p<0.05$.

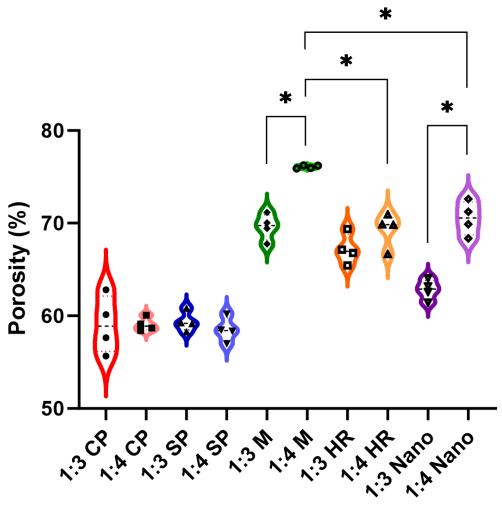


**Figure 4.16:** Porosity mean of the sample of every technique.

### *4.3.6 Porous scaffold mechanical tests*

In order to provide an additional parameter for the evaluation of the best scaffold, we decided to perform compression tests on each patch. The initial goal was to compare samples filled with distilled water, hydrogel and the mechanical behaviour of a PGS film with an upper layer of hydrogel. Although we had created both the hydrogel based on HA and the one based on PVA, for time limitation we opted for PVA by inserting it into a syringe with the sample and making it absorb creating the vacuum. The immersion in the sodium tetraborate completed the gelling of the hydrogel. After completing all the tests, when analysing the data, we realized that an error was made at the beginning, as the total displacement of the compression test exceeded the initial length of the test piece. The point is that the data showed the typical shape of an elastomeric, porous structure in a stress-strain plot and the device did not triggered an alarm for reaching the limit switch. The only reason I can find is that the water air interface, which has a strong surface tension, was pushing and preventing the rod from moving upwards, as if it was the resistance of the scaffold being squeezed. For reasons of time it was not possible to continue with other mechanical tests, which will be carried out outside the work of this thesis.

### *4.3.7 Final evaluation*

| | **Porosity** | **Minor Axis** | **Handling** | **Washing** |
|---|---|---|---|---|
| 1:3 SP | B | B | B | B |
| 1:4 SP | B | G | B | R |
| 1:3 CP | B | G | B | R |
| 1:4 CP | B | B | B | R |
| 1:3 M | G | G | G | G |
| 1:4 M | VG | G | G | VG |
| 1:3 HR | G | B | R | VG |
| 1:4 HR | G | R | R | VG |
| 1:3 Nano | R | VG | G | B |
| 1:4 Nano | G | G | G | B |

**Table 4.6:** Summary table of all parameters seen so far applied to the specimens. B = bad, R = regular, G = good, VG = very good. Porosity: B = <60%, 60 $\leq$ R $<$ 66%, 66% $\leq$ G $<$ 72%, VG $\geq$ 72%; Minor axis: B $<$ 15, 15 $\leq$ R $<$ 18, 18 $\leq$ G $<$ 21, VG $\geq$ 21 [$\mu$m]; Handling: B = bad shape, R = good shape, more time, G = good shape, regular time, VG not given; Washing: B $>$ 100, 75 $\leq$ R $\leq$ 100, 50 $\leq$ G $<$ 75, VG $<$ 50 [h].

The table 4.6 represents a subjective qualitative summary of the assessments made with all these experiments. Comparing the values CP and SP are the worst, while the values M are the best. Between the two mass ratios, what seems best is 1:4 because the porosity is higher and is the most significant parameter. This analysis is based on data obtained from individual samples. A more thorough analysis with several samples of the same species, especially between the two M and 1:4 Nano should be done. In addition, mechanical test data are missing, which could greatly affect the result because.

## 4.4 Electrospun membrane scaffold

### *4.4.1 Preparation of the PGS:ethanol compound*

The idea behind the preparation is that inside the syringe of the electrospinning there goes a compound formed by polymer and solvent, which during the ejection evaporates forming wires of only polymer that will be treated accordingly. PGS is soluble with ethanol, however the more cured it is, the less soluble it is. Therefore it was necessary to find a time of curing that would make it more accurate possible, without making it insoluble. Also it was necessary to find the right ratio PGS:ethanol.

PGS has been treated inside glass flasks to facilitate the procedure of dissolution in ethanol, aware that different treatment conditions would have meant not being able to rely on the traditional hours of treatment obtained by the method described in the paragraph 3.2. The polymer was weighed before being cured and after ethanol was removed after the curing process. The two weights were compared and a percentage of dissolution was estimated. The time of dissolution was initially unknown, so the vials were observed every 12 hours and it was found that 24 hours of dissolution were sufficient to obtain the final result.

Initially the PGS was placed in some 20 ml vials and treated with variable times between 10 hours and 30, at intervals of two hours, with every hour experiment with two w/v %, i.e. 10% and 15%. What we saw was that under 20 hours of treatment, all the prepolymer was dissolved, while over 20 hours in varying proportions descending from 70%, except for the specimen 20 h and 15% w/v, fig. 4.17. For this reason, more specific studies were carried out on 18 and 19 hours of treatment with concentration percentages between 10 and 25%. From this point onwards, since for a future experiment with electrospinning we needed more prepolymer, we opted to use larger vials and a proportion of mass that would allow us to maintain the same height of cured PGS in each vial.

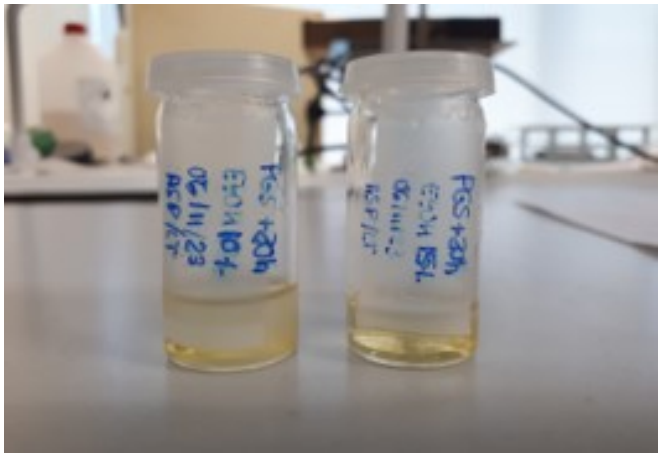

**Figure 4.17:** 20 h cured PGS in a ethanol solution. In the left there is the 10% w/v ratio, in the right the 15% one. We can see the difference between the PGS of almost the whole dissolved, and the other.

Then we analysed the samples with the DLS technique to see the molecules dimensions and the zeta potential dissolved in ethanol. We compared samples from 18 to 20 hours of curing with 10% w/v ratio. What we know about PGS production is that the glycerol and sebacic acid molecules

are very small, with dimensions within 20 nm. During the first condensation reaction, a polymer chain with variable length is obtained. What turns the prepolymer into elastomer is the chain crosslinking which is not a linear reaction, but starts at an unknown point that depends on the method of care.

The images show the dimensions at 18h and 20h using the larger vial. In the first (fig. 4.18a), the average size is 33.48 nm, while the second peak is much lower at 4738 nm. It is likely that the second region is due to the beginning of a chain crosslinking phase, which makes the chains larger. In the 20h sample (fig. 4.18a), in fact, it is noted that the average size of the molecules is higher, around 1294 nm, an index that is gradually increasing cross-linking. However, the structure of PGS during the crosslinking phase is unknown, so we cannot know for sure this information, despite being the most accredited hypothesis.

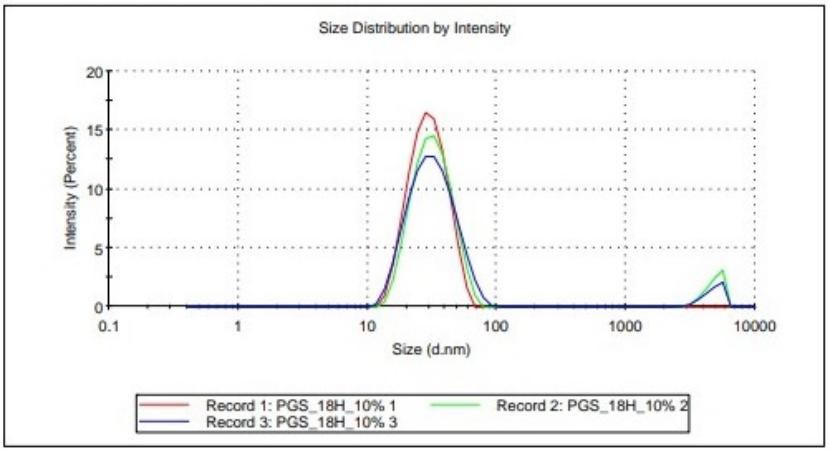


**(a)** PGS 18h cured. Peaks at 33.48 and 4738 nm.

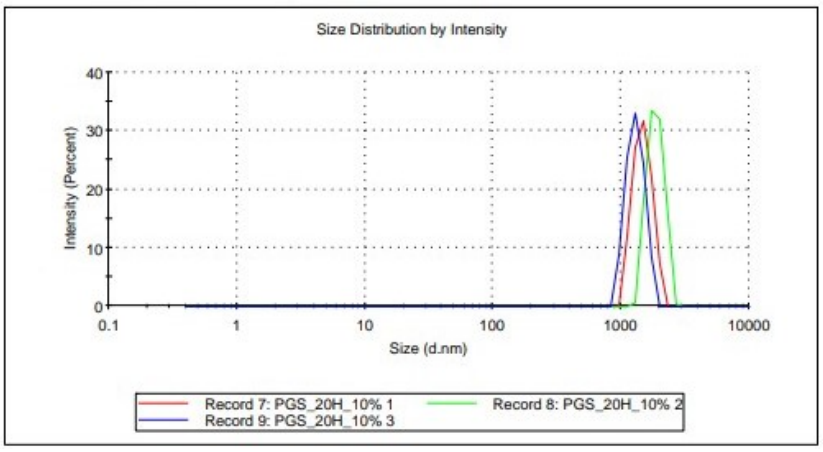


**(b)** PGS 20h cured.Peaks at 1136 nm.

**Figure 4.18:** Dimension distribution of PGS cured 18h and 20h through DLS technique. The three lines are due to three measurements of the Zetasizer.

In the following graphs there is the zeta potential. It gives us the potential of the ethanol solution. The potential of the 18-hour cured PGS solution provides us with a potential of $-1.14$ mV that tends to increase to $-0.47$ mV of the 20 hour specimen (fig. 4.18). The reason is related to the type of reaction between glycerol and sebacic acid. Esterification is a reaction that releases

protons of hydrogen. As molecules become esterified, they release more and more protons in the ethanol solution that will become more positive.

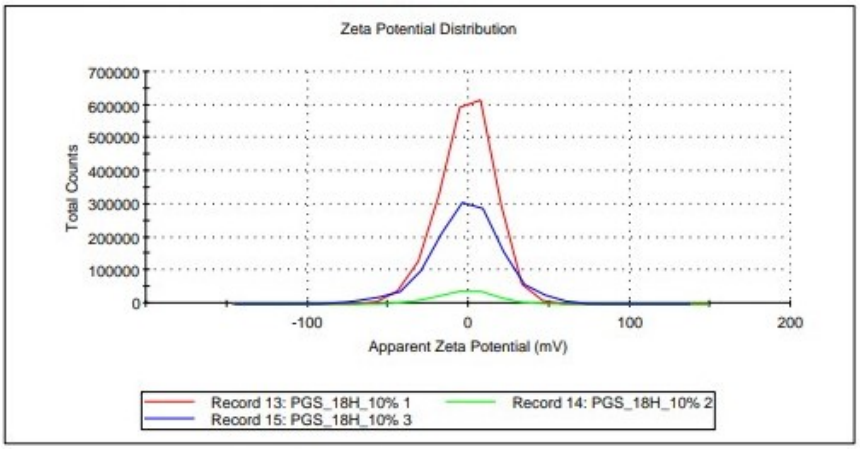


**(a)** PGS 18h cured. Peak at −1.14 mV.

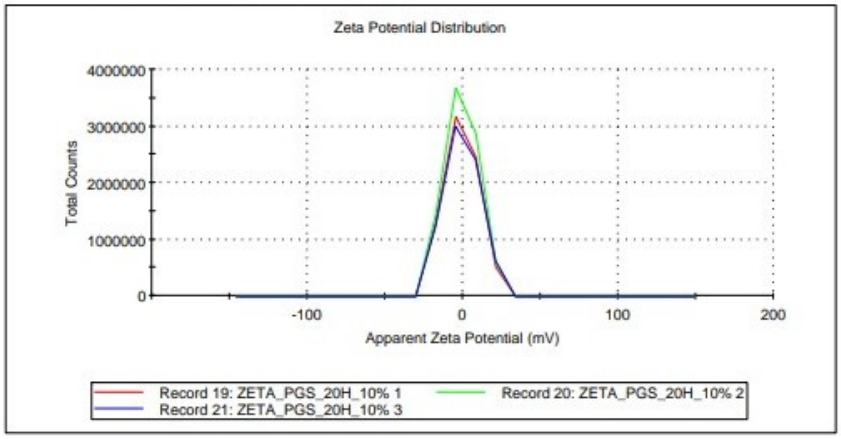


**(b)** PGS 20h cured. Peak at −0.47 mV.

**Figure 4.19:** Zeta potential of PGS cured 18h and 20h through DLS technique. The three lines are due to three measurements of the Zetasizer.

We compared the samples in the bigger vial with the ones in the smaller and we saw that the behaviour was the same with a discard of more than an hour. We continued to produce solutions using large vials aware that the increase in the hours of cured corresponded to the hours between 18 and 20 of the small vials. It would have been interesting to do DLS analysis at several hours of cured to obtain a complete curve of the size of the molecules. However the strong limitation of the technique is that PGS must be soluble and as it is treated it becomes insoluble.

### *4.4.2 Electrospinning results*

The next step was to place the PGS:ethanol compound in the electrospinning syringe. We started with 20h 15 % and noticed that there were no wires, but only small drops in the aluminium foil where they were thrown. We thought the problem was too much ethanol, so we tried to increase the PGS curing hours and raised the concentration rate to a maximum of 22h and 75%. At that point, because of the little time left to deliver the thesis and the time needed to search for new information in the bibliography, we have set aside the experiment that will be performed later.

In figure 4.20 PGS drops can be seen.

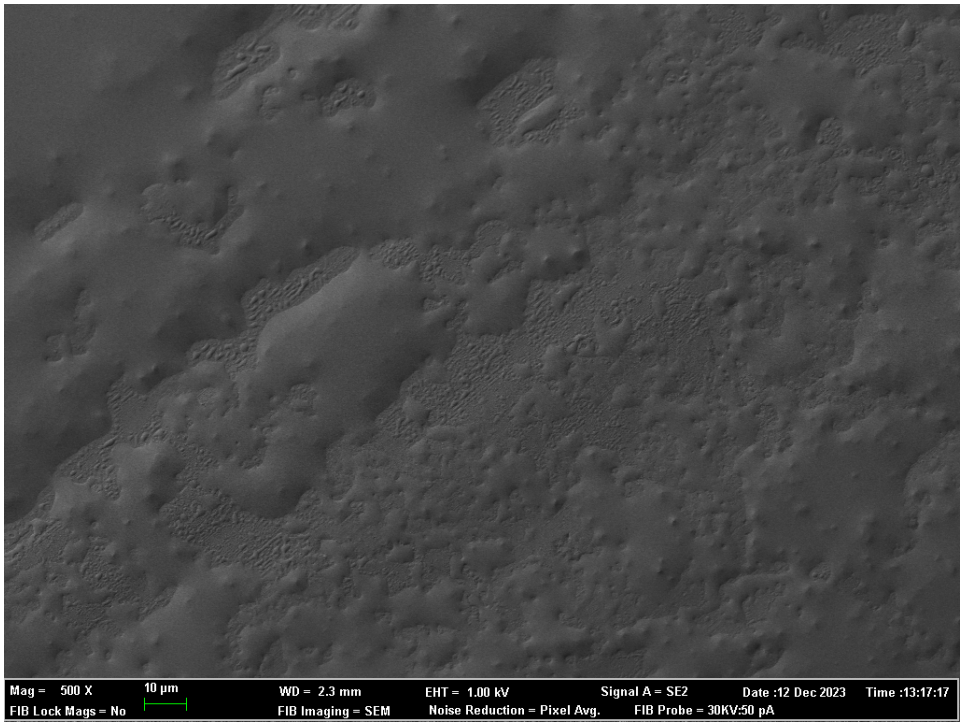


**Figure 4.20:** FESEM image of the aluminium paper with drops of PGS deposited with electrospinning technique. Scale bar = 10 $\mu$m.

# Chapter 5

# CONCLUSIONS

The work done in this thesis is not an end in itself, but is part of a larger project and the results obtained will be the basis on which someone else will continue. The objectives were various. On the one hand it was necessary to characterize the behavior of pure PGS. On the other it was necessary to create a structure that would serve as a basis for the insertion of a hydrogel that will be soaked with bioactive material that will be released for the treatment of particular wounds.

As for the characterization of PGS, it was necessary to understand if and how much PGS could be cured in a confined volume with little excess exposed to air. The results have shown that it undergoes a slightly stronger curing process either by increasing the curing time, or by lyophilising it in advance. We could think of studying the effect of each factor to create a curve, but the comparison with the standard method suggests that it would not make much sense because of the very long treatment time. One parameter that could be very interesting to study is the ratio of free surface to test specimen height. In this way the parameter becomes one and one could understand how to standardize the production of this polymer that holds too many production variables.

As regards the creation of a scaffold, two approaches have been tried: one porous by NaCl means of grains and one porous membrane obtained by electrospinning.

In the first, it was necessary to find the best combination of parameters for the scaffold to be porous enough to allow hydrogel injection, It had to have good interconnections between the pores to allow the passage of the biomolecules and had to maintain a good mechanical resistance to prevent it from deforming permanently in case of unintentional misuse by the patient. The results obtained have allowed us to optimize the methods for the creation, such as the filtration of the grains useful for the purpose, the minimum washing time of the scaffolds and the method of mixing the polymer with salt, that is, mixing them manually. The choice between the proportions fell on 1:4 because it provided more porosity. The use of additional methods to increase pore size has not been conclusive, however the lack of compression testing is an important factor that could influence the decision taken so far. The dimensions of the interconnections are acceptable on almost every sample, however to confirm the data we have to take into account the number

of them, which has not been calculated. For now the best method seems to be 1:4 M, but future assessments of missing experiments will need to be made to confirm this data.

Turning to the attempt to create a membrane of PGS by electrospinning, it turned out to be a partial failure. Further studies should be done to understand the cause of drops that could affect a change in concentration or curing of the polymer or solvent, such as tetrahydrofuran. But a step forward has been taken. Through the DLS you have had a first idea about what can be the healing interval in which the PGS begins to crosslinking. It would be interesting to deepen this study.

# Acronyms

**CP** Sample with pressure

**CSA** Cysteamine hydrochloride

**DLS** Dinamic Light Scattering

**DSC** Differential Scanning Calorimetry

**EDC-HCl** N-(3-(Dimethylaminopropyl)- N - ethylcarbodiimide hydrochloride

**EDTA** Ethylenediaminetetraacetic acid

**FESEM** Field Emission Scanning Electron Microscopy

**FTIR** Fourier Transform Infrared Spectroscophy

**HA** Hyaluronic Acid

**HR** Relative Humidity

**M** Sample with PGS and salt mixed manually

**Nano** Sample with nanosalt

**NHS** N-Hydroxysuccinimide

**NLC** Nanostructured Lipid Carrier

**PGS** Poli(Glycerol Sebacate)

**PLGA** Poli(Lactic Glycolic Acid)

**pPGS** prepolymer of PGS

**PVA** Poli(Vinil Alcohol)

**SP** Sample without pressure

**TMA** Thermal Mechanical Analysis

# Bibliography


[1] Wilfredo Lopez-Ojeda et al. "Anatomy, Skin (Integument)". In: *StatPearls Publishing* (2023) (cit. on pp. 3, 4).

[2] Hani Yousef, Mandy Alhajj, and Sandeep Sharma. "Anatomy, Skin (Integument), Epidermis". In: *StatPearl Publishing* (2023) (cit. on pp. 3, 4).

[3] Thomas M. Brown and Karthik Krishnamurthy. "Hystology, Dermis". In: *StatPearls Publishing* (2023) (cit. on p. 4).

[4] Donald L. Wise. *Biomaterials and Bioengineering Handbook*. C.R.C. Press, 2000 (cit. on p. 4).

[5] Ana Cristina de Oliveira Gonzalez et al. "Wound healing - A literature review". In: *An Bras Dermatol* (2016) (cit. on p. 4).

[6] Guo and Dipietro. "Factors affecting wound healing". In: *Journal of Dental Research* (2010) (cit. on p. 5).

[7] Rodney M. Donlan. "Biofilms: Microbial Life on Surfaces". In: *Emerging Infectious Deseases* (2002) (cit. on p. 5).

[8] Maria Kostakioti, Maria Hadjifrangiskou, and Scott J. Hultgren. "Bacterial Biofilms: Development, Dispersal,and Therapeutic Strategies in the Dawnof the Postantibiotic Era". In: *Cold Spring Harb Perspect Med* (2013) (cit. on p. 5).

[9] Jesaitis AJ et al. "Compromised host defense on Pseudomonas aeruginosa biofilms: Characterization of neutrophil and biofilm interactions". In: *J Immunol* (2003) (cit. on p. 5).

[10] Kimberly K. Jefferson, Donald A. Goldmann, and Gerald B. Pier. "Use of Confocal Microscopy To Analyze the Rate of Vancomycin Penetration through Staphylococcus aureus Biofilms". In: *Antimicrob Agents Chemother* (2005) (cit. on p. 5).

[11] Vuong Cand Voyich JM et al. "Polysaccharide intercellular adhesin (PIA) protects Staphylococcus epidermidis against major components of the human innate immune system". In: *Cell Microbiol* (2004) (cit. on p. 5).

[12] Seth D et al. "Burden of Skin Disease: Inequities and Innovations". In: *Curr Dermatol Rep.* (2017) (cit. on p. 5).

[13] C. Flohr and R. Hay. "Putting the burden of skin diseases on the global map". In: *Br J Dermatol* (2021) (cit. on p. 5).

[14] *Hartmann Hydrocoll Technical Data Sheet* (cit. on p. 5).

[15] Ripolin A et al. "Successful application of a large microneedle patches by human volunteers". In: *Int J Pharm* (2017) (cit. on p. 5).

[16] Ziesmer J et al. "Vancomycin-Loaded Microneedle Arrays against Methicillin-Resistant Staphylococcus Aureus Skin Infections". In: *Adv Mater Technol* (2021) (cit. on p. 5).

[17] Chi J et al. "Antibacterial and angiogenic chitosan microneedle array patch for promoting wound healing". In: *Bioactive Materials* (2020) (cit. on p. 5).

[18] Li C et al. "Flexible Nanoholey Patches for Antibiotic-Free Treatments of Skin Infections". In: *ACS Appl Mater Interfacer* (2012) (cit. on p. 6).

[19] Vollono L et al. "Potential of Curcumin in Skin Disorders". In: *Nutrients* (2019) (cit. on p. 6).

[20] Thangapazham RL, Sharma A, and Maheshwari RK. "Beneficial role of curcumin in skin diseases". In: *Adv Exp Med Biol* (2007) (cit. on p. 6).

[21] Duplessis CA and Biswas B. "A Review of Topical Phage Therapy for Chronically Infected Wounds and Preparations for a Randomized Adaptive Clinical Trial Evaluating Topical Phage Therapy in Chronically Infected Diabetic Foot Ulcers". In: *Antibiotics* (2020) (cit. on p. 6).

[22] Markoishvili K et al. "A novel sustained-release matrix based on biodegradable poly(ester amide)s and impregnated with bacteriophages and an antibiotic shows promise in management of infected venous stasis ulcers and other poorly healing wounds". In: *Int J Dermatol* (2002) (cit. on p. 6).

[23] Jault P et al. "Efficacy and tolerability of a cocktail of bacteriophages to treat burn wounds infected by Pseudomonas aeruginosa (PhagoBurn): A randomized, controlled, double-blind phase 1/2 trial." In: *Lancet. Infect Dis* (2019) (cit. on p. 6).

[24] Guo B et al. "Haemostatic materials for wound healing applications". In: *Nat Rev Chem* (2021) (cit. on p. 7).

[25] Yadong Wang et al. “A tough biodegradable elastomer”. In: *Biotech Nature* (2002) (cit. on p. 8).

[26] Yadong Wang et al. “Poly(Glycerol Sebacate) in Tissue Engineering and Regenerative Medicine”. In: *Material Matters* (2016) (cit. on p. 8).

[27] Ranjana Rai et al. “Synthesis, properties and biomedical applications of poly(glycerolsebacate) (PGS): A review”. In: *Progress in Polymer Science* (2012) (cit. on pp. 8, 9).

[28] Minoru Nagata et al. “Synthesis, characterization, and enzymatic degradation of network aliphatic copolyesters”. In: *Journal of Polymer Science* (2000) (cit. on p. 8).

[29] Álvaro Conejero-García et al. “Correlating synthesis parameters with physicochemicalproperties of poly(glycerol sebacate)”. In: *European Polymer Journal* (2017) (cit. on p. 8).

[30] Rubén Martín-Cabezuelo. “Monitoring of the parameters of synthesis of poly(glycerol sebacate) and influence on the physicochemical and biological properties of its elastomer”. PhD thesis. Universitat Politècnica de València, 2020 (cit. on pp. 8, 18).

[31] Xinda Li et al. “Criteria for Quick and Consistent Synthesis of Poly(glycerol sebacate)for Tailored Mechanical Properties”. In: *Biomac* (2015) (cit. on pp. 8, 9).

[32] Wang Y, Kim YM, and Langer R. “In vivo degradation characteristics of poly(glycerol sebacate)”. In: *J Biomed Mater Res* (2003) (cit. on pp. 9, 10).

[33] Lena Vogt et al. “Poly(Glycerol Sebacate) in Biomedical Applications-A Review of the Recent Literature”. In: *Adv Healthc Mater* (2021) (cit. on pp. 9, 11).

[34] J.W. Kuo and G.D. Prestwich. “Hyaluronic Acid”. In: *Comprehensive Biomaterials* (2011) (cit. on p. 10).

[35] Tayser Sumer Gaaz et al. “Properties and Applications of Polyvinyl Alcohol, Halloysite Nanotubes and Their Nanocomposites”. In: *Molecules* (2015) (cit. on p. 12).

[36] Masoumi N et al. “Tri-layered elastomeric scaffolds for engineering heart valve leaflets”. In: *Biomaterials* (2014) (cit. on p. 12).

[37] Ravichandran R et al. “Poly(Glycerol sebacate)/gelatin core/shell fibrous structure for regeneration of myocardial infarction”. In: *Tissue Eng A* (2011) (cit. on p. 12).

[38] Vogt L et al. “Electrospun Zein Fibers Incorporating Poly(glycerol sebacate) for Soft Tissue Engineering”. In: *Nanomater* (2018) (cit. on p. 12).

[39] Guillermo Vilariño-Feltrer et al. “The effect of salt fusion processing variables on structural, physicochemical and biologicalproperties of poly(glycerol sebacate) scaffolds”. In: *International Journal of Polymeric Materials andPolymeric Biomaterials* (2020) (cit. on p. 22).

[40] Lewis Greenspan. "Humidity Fixed Points of Binary Saturated Aqueous Solutions". In: *J Res Natl Bur Stand A Phys Chem* (1977) (cit. on p. 24).

[41] Shaoquan Bian et al. "The self-crosslinking smart hyaluronic acid hydrogels as injectablethree-dimensional scaffolds for cells culture". In: *Colloids and Surfaces B: Biointerfaces* (2016) (cit. on p. 29).

[42] Ellman G.L. "Tissue sulfhydryl groups". In: *Arch Biochem Biophys* (1959) (cit. on p. 30).

# Part II

# BUDGET

| PROJECT PRICE TABLE<br>ITEMS PRICE LIST | | |
|---|---|---|
| **CODE** | **Item** | **Price per unit** |
| | **Work Force** | |
| WF.DIR | h Project Director | 22.00 € |
| WF.INV | h Research inspector | 13.50 € |
| WF.TLAB | h Laboratory technician | 12.30 € |
| | **Machinery** | |
| MAC.SC | h Mettler Toledo scale AX205 | 0.01 € |
| MAC.BOM | h Vacuum pump Vacubrand | 0.12 € |
| MAC.BZM | h Mettler Toledo AE-240 | 0.56 € |
| MAC.DES | h Vacuum dried JP Selecta | 0.02 € |
| MAC.HOR | h Oven JP Selecta | 0.18 € |
| MAC.DSC | h DSC PerkinElmer 8000 | 1.55 € |
| MAC.FTIR | h Platinum ATR ALPHA | 0.23 € |
| MAC.FE1 | h Zemini Ultra55 | 25.00 € |
| MAC.TMA | h TMA SS6000 | 0.53 € |
| MAC.FE2 | h Leica EM MED020 | 10.00 € |
| MAC.ZET | h Zetasizer NanoZ590 | 0.45 € |
| MAC.SIE | h Sieving Machine Filtra | 0.11 € |
| MAC.FRE | h Freeze-Drier Telstar LyoQue | 0.66 € |
| MAC.ELS | h Electrospinning machine | 0.33 € |
| MAC.SCA | h Digiterm 200 | 0.05 € |
| MAC.CON | h Conductimeter | 0.09 € |
| | | |
| | **Material** | |
| MAT.AP | u Aluminium paper | 1.49 € |
| MAT.CHO | kg Chondroitin sulfate sodium salt from shark cartilage | 282.00 € |
| MAT.CLI | u Clip | 0.10 € |
| MAT.CUT | u Cutter | 0.10 € |
| MAT.CYS | L Cysteamine hydrochloride / CSA·HCl | 39.56 € |
| MAT.CYT | m Cytiva Sephacryl™ S-500 High Resolution Media | 201.00 € |
| MAT.DI- | kg Di-Sodium hydrogen phosphate dodecahydrate Na2HPO4•12H2O | 27.40 € |
| MAT.DW | L Distilled water | 0.50 € |
| MAT.DM | u Dust mask | 2.50 € |
| MAT.EPP | u Eppendorf | 0.01 € |
| MAT.ETH | L Ethanol | 0.50 € |
| MAT.FP | u Filter paper | 0.01 € |
| MAT.GM | u Gas Mask | 75.00 € |
| MAT.GP | u Glass plate | 1.00 € |
| MAT.GLY | L Glycerol | 71.80 € |
| MAT.GC | u Graduated cylinder 200 ml | 12.32 € |
| MAT.HYA | kg Hyaluronic acid sodium salt from streptococcus equi sp. | 310.00 € |
| MAT.LM | u Laboratory coat | 57.00 € |
| MAT.LG | u Latex gloves | 0.03 € |
| MAT.MS | u Metal spatula | 3.50 € |
| MAT.MQW | L milliQ water | 3.45 € |
| MAT.EDC | u N-(3-Dimethylaminopropyl)-N'-ethylcarbodiimide hydrochloride/ EDC | 50.00 € |

| | | |
|---|---|---|
| MAT.NAC | kg NaCl | 0.89 € |
| MAT.N-H | kg N-Hydroxysuccinimide / 1-Hydroxy-2,5-pyrrolidinedione / HOSu | 29.40 € |
| MAT.NM | u Nitrogen bomb | 50.00 € |
| MAT.PT | u Pipette tip | 29.31 € |
| MAT.PS | u Plastic spatula | 2.00 € |
| MAT.POL | L Polyvinyl Cloride | 312.00 € |
| MAT.SA | kg Sebacic acid | 98.38 € |
| MAT.SC | kg Sodium chloride | 142.00 € |
| MAT.SOD | kg Sodium dihydrogen phosphate 2-hydrate NaH2PO4•2H2O | 39.70 € |
| MAT.SOD | kg Sodium Tetraborate | 21.00 € |
| MAT.SPE | m Spectra for 3 MWCO 3500 width 45 mm | 336.00 € |
| MAT.SPE | m Spectra-Por® Float-A-Lyzer® G2 blue, 10 ml, MWCO 100 kDa | 179.00 € |
| MAT.TF | m Teflon film | 6.50 € |
| MAT.TM | u Teflon mould | 66.00 € |
| MAT.TG | u Thermic gloves | 1.49 € |
| MAT.TRO | u Troquel | 3.20 € |
| MAT.TUP | u Tupperware | 1.50 € |
| MAT.VIA | u Vial | 0.50 € |

| PROJECT PRICE TABLE<br>COSTS | | | | |
|---|---|---|---|---|
| **CODE** | **Item** | **Unit price** | **Units** | **Total** |
| | **Creation of PGS films** | | | |
| WF.TLAB | Laboratory technician | 12.30 € | 20 | 246.00 € |
| MAC.BOM | Vacuum pump Vacubrand | 0.12 € | 300 | 36.00 € |
| MAC.HOR | Oven JP Selecta | 0.18 € | 1200 | 216.00 € |
| MAT.CLI | Clip | 0.10 € | 20 | 2.00 € |
| MAT.CUT | Cutter | 0.10 € | 2 | 0.20 € |
| MAT.GP | Glass plate | 1.00 € | 5 | 5.00 € |
| MAT.GLY | Glycerol | 71.80 € | 0.624 | 44.80 € |
| MAT.NM | Nitrogen bomb | 50.00 € | 0.2 | 10.00 € |
| MAT.SA | Sebacic acid | 98.38 € | 0.22 | 21.64 € |
| MAT.TF | Teflon film | 6.50 € | 1 | 6.50 € |
| MAT.TG | Thermic gloves | 1.49 € | 1 | 1.49 € |
| | | | | **589.64 €** |
| | **Physical-chemical characterization** | | | |
| WF.TLAB | Laboratory technician | 12.30 € | 40 | 492.00 € |
| MAC.BZM | Mettler Toledo AE-240 | 0.56 € | 20 | 11.20 € |
| MAC.DSC | DSC PerkinElmer 8000 | 1.55 € | 24 | 37.20 € |
| MAC.FTIR | Platinum ATR ALPHA | 0.23 € | 6 | 1.38 € |
| MAT.EPP | Eppendorf | 0.01 € | 50 | 0.50 € |
| MAT.MS | Metal spatula | 3.50 € | 1 | 3.50 € |
| MAT.PS | Plastic spatula | 2.00 € | 1 | 2.00 € |
| MAT.TRO | Troquel | 3.20 € | 1 | 3.20 € |
| | | | | **550.98 €** |
| | **Porous scaffold production** | | | |
| WF.TLAB | Laboratory technician | 12.30 € | 245 | 3,013.50 € |
| MAC.SC | Mettler Toledo scale AX205 | 0.01 € | 10 | 0.10 € |
| MAC.BOM | Vacuum pump Vacubrand | 0.12 € | 150 | 18.00 € |
| MAC.DES | Vacuum dried JP Selecta | 0.02 € | 48 | 0.96 € |
| MAC.HOR | Oven JP Selecta | 0.18 € | 100 | 18.00 € |
| MAC.SIE | Sieving Machine Filtra | 0.11 € | 30 | 3.30 € |
| MAC.CON | Conductimeter | 0.09 € | 6 | 0.54 € |
| MAT.DW | Distilled water | 0.50 € | 20 | 10.00 € |
| MAT.GLY | Glycerol | 71.80 € | 0.03 | 2.15 € |
| MAT.GC | Graduated cylinder 200 ml | 12.32 € | 1 | 12.32 € |
| MAT.MS | Metal spatula | 3.50 € | 1 | 3.50 € |
| MAT.MQW | milliQ water | 3.45 € | 50 | 172.50 € |
| MAT.NAC | NaCl | 0.89 € | 1 | 0.89 € |
| MAT.SA | Sebacic acid | 98.38 € | 0.07 | 6.89 € |
| MAT.SOD | Sodium Tetraborate | 21.00 € | 0.01 | 0.21 € |
| MAT.TM | Teflon mould | 66.00 € | 5 | 330.00 € |
| MAT.TUP | Tupperware | 1.50 € | 6 | 9.00 € |
| MAC.FE1 | Zemini Ultra55 | 25.00 € | 10 | 250.00 € |
| MAC.FE2 | Leica EM MED020 | 10.00 € | 2 | 20.00 € |
| | | | | **3,871.86 €** |
| | **Electrospun membrane production** | | | |
| WF.INV | Research inspector | 13.50 € | 3 | 40.50 € |
| WF.TLAB | Laboratory technician | 12.30 € | 150 | 1,845.00 € |
| MAC.SC | Mettler Toledo scale AX205 | 0.01 € | 1 | 0.01 € |

| | | | | |
|---|---|---|---|---|
| MAC.HOR | Oven JP Selecta | 0.18 € | 400 | 72.00 € |
| MAC.ZET | Zetasizer NanoZ590 | 0.45 € | 4 | 1.80 € |
| MAC.ELS | Electrospinning machine | 0.33 € | 3 | 0.99 € |
| MAT.ETH | Ethanol | 0.50 € | 0.26 | 0.13 € |
| MAT.GLY | Glycerol | 71.80 € | 0.13 | 9.33 € |
| MAT.MS | Metal spatula | 3.50 € | 1 | 3.50 € |
| MAT.VIA | Vial | 0.50 € | 50 | 25.00 € |
| | | | | **1,998.26 €** |
| | **Hydrogel production** | | | |
| WF.TLAB | Laboratory technician | 12.30 € | 15 | 184.50 € |
| MAC.SCA | Digiterm 200 | 0.05 € | 48 | 2.40 € |
| MAT.CHO | Chondroitin sulfate sodium salt from shark cartilage | 282.00 € | 0.05 | 14.10 € |
| MAT.CYS | Cysteamine hydrochloride / CSA·HCl | 39.56 € | 0.03 | 1.19 € |
| MAT.CYT | Cytiva Sephacryl™ S-500 High Resolution Media | 201.00 € | 0.06 | 12.06 € |
| MAT.DI- | Di-Sodium hydrogen phosphate dodecahydrate Na2HPO4•12H2O | 27.40 € | 0.01 | 0.27 € |
| MAT.DW | Distilled water | 0.50 € | 0.5 | 0.25 € |
| MAT.EPP | Eppendorf | 0.01 € | 5 | 0.05 € |
| MAT.HYA | Hyaluronic acid sodium salt from streptococcus equi sp. | 310.00 € | 0.05 | 15.50 € |
| MAT.EDC | N-(3-Dimethylaminopropyl)-N'-ethylcarbodiimide hydrochloride/ EDC | 50.00 € | 0.04 | 2.00 € |
| MAT.N-H | N-Hydroxysuccinimide / 1-Hydroxy-2,5-pyrrolidinedione / HOSu | 29.40 € | 0.02 | 0.59 € |
| MAT.PT | Pipette tip | 29.31 € | 1 | 29.31 € |
| MAT.SC | Sodium chloride | 142.00 € | 0.02 | 2.84 € |
| MAT.SOD | Sodium dihydrogen phosphate 2-hydrate NaH2PO4•2H2O | 39.70 € | 0.01 | 0.40 € |
| MAT.SPE | Spectra for 3 MWCO 3500 width 45 mm | 336.00 € | 0.1 | 33.60 € |
| MAT.SPE | Spectra-Por® Float-A-Lyzer® G2 blue, 10 ml, MWCO 100 kDa | 179.00 € | 0.2 | 35.80 € |
| | | | | **334.86 €** |
| | **Security devices** | | | |
| MAT.GM | Gas Mask | 75.00 € | 1 | 75.00 € |
| MAT.GP | Glass plate | 1.00 € | 1 | 1.00 € |
| MAT.LM | Laboratory coat | 57.00 € | 1 | 57.00 € |
| MAT.LG | Latex gloves | 0.03 € | 1 | 0.03 € |
| MAT.TG | Thermic gloves | 1.49 € | 1 | 1.49 € |
| | | | | **134.52 €** |
| | **Periodical Reunions** | | | |
| WF.DIR | Project Director | 22.00 € | 10 | 220.00 € |
| WF.INV | Research inspector | 13.50 € | 10 | 135.00 € |
| WF.TLAB | Laboratory technician | 12.30 € | 10 | 123.00 € |
| | | | | **478.00 €** |
| | **TOTAL** | | | **7,958.12 €** |

| PROJECT PRICE TABLE<br>SUMMARY | | |
|---|---|---|
| **Description** | | **Cost** |
| Creation of PGS films | | 589.64 € |
| Physical-chemical characterization | | 550.98 € |
| Porous scaffold production | | 3,871.86 € |
| Electrospun membrane production | | 1,998.26 € |
| Hydrogel production | | 334.86 € |
| Security devices | | 134.52 € |
| Periodical Reunions | | 478.00 € |
| **MATERIAL DIRECT COSTS** | | **7,958.12 €** |
| General expenses | 13% | 1,034.56 € |
| Industrial profit | 6% | 477.49 € |
| **TOTAL CONTRACT EXECUTION** | | **9,470.16 €** |
| V.A.T | 21% | 1,988.73 € |
| **TOTAL BUDGET** | | **11,458.89 €** |